A WSR-88D Assessment of Tropical Cyclone Outer Rainband Tornadoes

SCOTT M. SPRATT AND DAVID W. SHARP

NEXRAD Weather Service Office, National Weather Service, Melbourne, Florida

PAT WELSH AND AL SANDRIK

NEXRAD Weather Service Office, National Weather Service, Jacksonville, Florida

FRANK ALSHEIMER AND CHARLIE PAXTON

NEXRAD Weather Service Office, National Weather Service, Tampa Bay, Florida

(Manuscript received 5 January 1996, in final form 15 April 1997)

ABSTRACT

As part of the National Weather Service (NWS) Modernization and Restructuring Program, WSR-88D (NEXRAD) Doppler radar installation has been completed at each Weather Service Office in Florida. Recently, this powerful new tool provided unique opportunities for Jacksonville, Tampa Bay, and Melbourne NEXRAD Weather Service Office personnel to investigate tropical cyclone (TC) rainbands for evidence of tornadogenesis.

This study provides a radar-based analysis of known tornadic mesocyclones associated with two mature tropical cyclones that were *not* landfalling in the vicinity of the tornado occurrence, namely, Tropical Storm Gordon (1994) and Hurricane Allison (1995). Based on successful NEXRAD sampling strategies, detailed analyses of storm-scale reflectivity and velocity signatures are conducted in the context of establishing preliminary critical criteria for use in the tornado detection and warning process. Important characteristics were found to include detection of discrete, small diameter >50 dBZ echos collocated with storm-relative rotational velocities of 6.5–15 m s^{-1}. Rotational features, although often subtle, were identifiable for an average of 30 min prior to tornado production, with total durations of 1–2 h. Near the time of tornado touchdown, the core diameter of the low-level circulation couplets contracted to approximately 1.85 km (1 n mi), leading to an associated increase of shear across the circulation to 0.010 s^{-1} or greater.

A comparison between the well-studied Great Plains tornadic supercell and the observed TC-tornado cells revealed a common trait of persistence. While the average depth of rotation associated with the TC-tornado cells (3.5 km) was much more shallow than their midwest counterparts, the ratio of depth of rotation to storm top were comparable. However, the shallow depth and weaker detectable rotation of the TC (tornadic) mesocyclones greatly reduced the detection capability of the current WSR-88D mesocyclone algorithm when compared to identification of traditional supercells.

Based upon the analyzed data, the authors offer several recommendations to assist operational radar meteorologists with the challenging task of detecting outer rainband tornadoes. Additionally, the authors propose a new WSR-88D scan strategy (volume coverage pattern, VCP) that would provide additional low-level slices in lieu of several current upper-elevation angles. This new VCP would facilitate improved vertical sampling at lower heights where TC mesoscale circulations are most likely to be detected.

1. Introduction

In the United States, tornadoes account for as much as 10% of the total deaths associated with tropical cyclones (Novlan and Gray 1974). Most tropical cyclone (TC) tornadoes occur within 24 h of landfall and are favored within a sector 0°–120° in azimuth, relative to true north from the cyclone center (Hill et al. 1966; Novlan and Gray 1974; Gentry 1983). By a large percentage, tropical cyclones landfalling from the Gulf of Mexico produce more tornadoes than Atlantic storms. This is also true for Florida events, where Hagemeyer and Hodanish (1995) found that 87% of tornado-producing tropical cyclones have historically approached from the Gulf of Mexico, placing the state in the preferred sector.

Gentry (1983) and Weiss (1987) found a bimodal distribution of tropical cyclone tornadoes with respect to range from the cyclone center. ''Core'' tornadoes occur within inner rainbands or in the eyewall, while the optimum range for ''outer rainband'' tornadoes is 200–400 km from the center, but they can occur at even greater distances. Weiss (1987) found that more than

Corresponding author address: Scott M. Spratt, National Weather Service, 421 Croton Road, Melbourne, FL 32935.
E-mail: scott.spratt@noaa.gov

74% of postlandfall tornado occurrences reported from 1964 to 1983 were associated with outer band convection, while in a study of Florida tornadoes associated with tropical cyclones between 1882 and 1994, Hagemeyer and Hodanish (1995) stated that 25 of 61 cases involved tornadoes that occurred on the ''outer fringes of systems.'' It is at these greater distances from the TC center, where the severe weather awareness may not be high, that tornadoes could be the primary threat (Weiss 1987; McCaul 1991).

On several occasions airborne Doppler radars aboard National Oceanic and Atmospheric Administration research aircraft have detected small-scale vortices (also referred to as mesovorticies or mesocyclones) within convective eyewall bands of intensifying strong hurricanes (Marks and Houze 1984; Black and Marks 1991; Willoughby and Black 1996). Stewart and Lyons (1996) more recently observed similar features during a WSR-88D interrogation of Tropical Storm Ed's 1993 landfall on Guam. While these inner rainband vorticies can be significant to the local warning meteorologist (Fujita 1993; Wakimoto and Black 1994), this paper will strictly focus upon outer rainband mesocyclones and associated tornadoes, as observed during TC's Gordon and Allison.

The occurrence of multiple tornadoes, or tornado outbreaks, associated with tropical cyclones has been a problem facing operational meteorologists for some time. Multiple tornadoes are often observed to be associated with the strongest convective cells within the outer rainbands (Hill et al. 1966; Fujita et al. 1972), where convergence and vorticity gradients are the greatest. Several studies (Novlan and Gray 1974; Gentry 1983; Weiss 1985) have described characteristics of the tropical cyclone environment that have occasionally become conducive for the occurrence of multiple tornado events. McCaul (1991) analyzed 1296 rawinsonde observations (raobs) that were within 3 h and 200 km of an observed TC-tornado and computed the spatial distribution of potential buoyant energy (or convective available potential energy, CAPE) and 0–3-km storm-relative helicity (SRH), which provides an estimate of a cell's potential of developing a rotating updraft. Results showed the SRH was maximized to the right of the cyclone with increasing CAPE at greater distances. Restricting raobs to those within 2 h and 40 km of hurricane-spawned tornadoes and made on the outer side of any rainbands in which the tornadoes were embedded, McCaul produced a composite of 10 soundings with a buoyancy (CAPE) of only 253 J kg^{-1} and an approximate SRH of 300 m^2 s^{-2}. In a comparison with nontropical tornado environments, Bluestein and Jain (1985) found CAPE values 10 times larger for Oklahoma supercells, and Davies-Jones et al. (1990) correlated SRH values of 150–300 m^2 s^{-2} with weak tornadoes (F0–F1) and values above 300 with strong to violent tornadoes ($\geq$ F2). Novlan and Gray (1974) suggested that strong vertical shear was the largest contributing factor to the genesis of tornadic cells within tropical cyclones and that buoyant instability played only a minor role. In model simulations of TC-spawned supercells, Weisman and McCaul (1995) found that the upward dynamic pressure gradient force contributed about three times as much to the updraft speed as buoyancy. Collectively, these sources have served to raise the level of understanding and anticipation of the TC-tornado threat through climatological patterns, statistics, and buoyancy/shear assessments.

Even with an increased recognition of favorable synoptic-scale TC-tornado environments, many of these tornadoes still occur without official National Weather Service (NWS) warnings or with little (or negative) lead time. To increase warning skill, an improved understanding of storm-scale characteristics and radar interpretation utilizing WSR-88 Doppler technology is essential. This can be achieved by further defining the structure and evolution of TC–tornadoes through model simulation efforts (e.g., McCaul 1990; Weisman and McCaul 1995) and through case study analyses (e.g., McCaul 1987; Snell and McCaul 1993; Zubrick and Belville 1993; Cammarata et al. 1996). Specific to outer band tornadogenesis, McCaul (1987), McCaul et al. (1993), and Snell and McCaul (1993) have made significant contributions via the analysis of data from several 10-cm/WSR-57 radars and a Doppler-enhanced 5-cm/WSR-74C radar during the postlandfall tornado outbreaks associated with Hurricane's Danny (1985) and Andrew (1992). The present paper will build upon the foundation established by the previously sited authors.

Radar signatures of multiple tornadic mesocyclones associated with banded convection of Tropical Storm Gordon (1994) and Hurricane Allison (1995) will be investigated using products from three Florida 10-cm/WSR-88Ds. During each event, outer band convection resulted in an ''outbreak'' of tornadoes as defined by Hagemeyer and Hodanish (1995), within a highly sheared and weakly buoyant environment. The majority of these tornadoes occurred very near the coast and were weak (F0–F1) with short tracks; however, a brief F2 tornado did produce numerous casualties and considerable destruction.

Section 2 will provide a background of some sampling considerations of the WSR-88D related to the observation of tropical, low-topped rotational cells. Sections 3 through 6 will present short synoptic overviews and storm-scale discussions of each tornado event by examining the temporal trends of several radar-observed parameters throughout the life cycle of four individual severe cells. Rotational aspects of each cell will be assessed in a storm-relative reference frame, along with a discussion of the performance of the current mesocyclone (M) algorithm (WSR-88D build 8.0; 1995). The effectiveness of other products, including vertically integrated liquid (VIL), echo tops

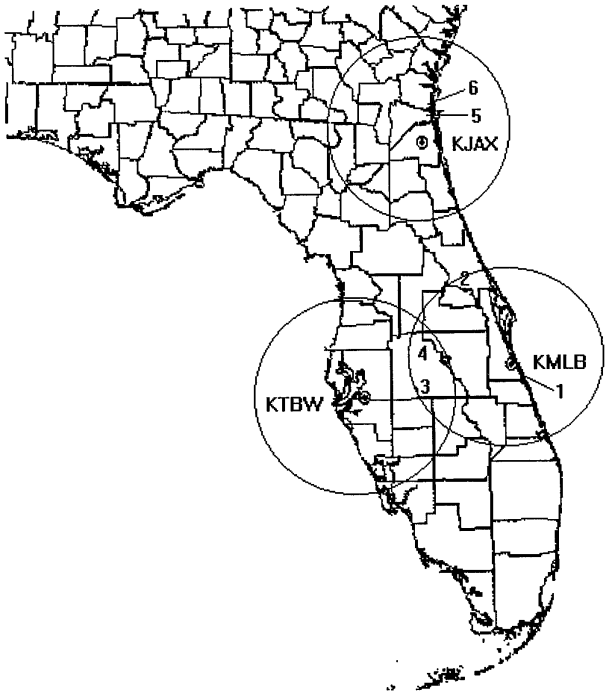

FIG. 1. Map of the Florida peninsula and southern Georgia with locations of the Jacksonville (KJAX), Tampa Bay (KTBW), and Melbourne (KMLB) WSR-88D sites. Range rings are indicated around each radar site at radius of 111 km (60 n mi). Tornadoes discussed within the text are labeled chronologically: Barefoot Bay (1), Iron Bend (2), Polk County at Lake Wales (3), Polk County at Haines City (4), Florida–Georgia state line (5), and St. Marys (6).

(ET), and spectrum width (SW) will be examined. Section 7 will review the most noteworthy radar-based observations, describe several recently employed analysis techniques, and introduce some preliminary criteria for the detection of TC-tornadoes. Several recommendations will also be made to improve the warning decision process for radar meteorologists tasked with TC outer rainband interrogation, and a proposal for a new WSR-88D volume coverage pattern (VCP) will be offered. The study will conclude by summarizing the similarities and differences of the detected circulations and compare their characteristics with those of Great Plains supercells of average dimension.

2. The WSR-88D and related sampling considerations

a. Radar data

The WSR-88D offers distinct advantages over previous network radars with improved sensitivity, greater resolution, and Doppler capabilities. With the digital base data stream connected to a computer processor, meteorological algorithms additionally furnish many derived products. The postprocessed (level IV) archived data used throughout this study were obtained from radars located at the Jacksonville (KJAX), Tampa Bay (KTBW), and Melbourne (KMLB) NWS offices (Fig. 1). These data represent the set of products used in real time by the local radar warning offices. For a complete description of all available WSR-88D products, see Klazura and Imy (1993) and the *Federal Meteorological Handbook 11*: Part C (OFCM 1991).

In precipitation mode, the WSR-88D gathers base moment data according to one of two prescribed VCPs. The scan strategy designated VCP 21 offers data from 9 elevation angles every 6 min, while VCP 11 offers data from 14 elevation angles every 5 min. During Gordon, the KMLB radar operated in VCP 11 during the first event (Barefoot Bay), while VCP 21 was used throughout the second case (Iron Bend). During all Allison events, VCP 21 was employed by both the KTBW and KJAX radars.

b. Aspect ratio and radar horizon sampling considerations

Recently, McCaul and Weisman (1996) numerically simulated low-topped supercells that had characteristics consistent with those observed by radar within TC environments. The simulations revealed that although the low-topped cells may contain updrafts that rival or exceed the intensity of Great Plains supercells, overall they exhibit a pronounced reduction of horizontal and vertical size. When a greater than average (TC environment) buoyancy was input to the model, intense and long-lived supercells resulted with well-defined hook echoes and bounded weak-echo regions, similar to those observed during TCs Danny (McCaul 1987), Andrew (Snell and McCaul 1993), and Beryl (Cammarata et al. 1996). However, when using buoyancy values more typical of TC environments, relatively weak (low level) rotational velocities and less pronounced reflectivity signatures resulted, which would pose a dilemma for meteorologists who must issue severe weather warnings to the public (McCaul and Weisman 1996). Understanding the behavior and characteristics of these more subtle features will help the radar operator make conscious decisions regarding tornadic potential and subsequent warnings without more traditionally definitive radar signatures.

Atmospheric sampling by radar is subject to two physical limitations, ''aspect ratio'' and ''radar horizon'' (Burgess et al. 1993). The effects of both limitations are accentuated for features like TC mesocyclones, which often possess small-diameter, shallow circulations. Basically, a mesocyclone core with a fixed diameter is less likely to be clearly resolved at greater distances from the radar due to beam broadening (increasing aspect ratio). Given the 1° beamwidth of the WSR-88D, a mesocyclone diameter of >3.5 km (>2 n mi) should be at least partially detected out to 222 km from the radar; however, a diameter of >1.85 km (1 n mi) would only be resolvable out to 111 km. In situations where the aspect ratio becomes large, ex-

amination of spectrum width may help locate mesocyclones and tornadoes as it provides a measure of the variability of the mean radial velocity estimates due to wind shear and turbulence (Klazura and Imy 1993). For example, at distances where both the inbound and outbound components of a circulation occur within a single beamwidth, detection of the rotational signature may be absent (as radial velocities average toward zero); however, detected SW values should be greater relative to surrounding cells.

The second restraint upon radar detection efficiency takes place due to the shallow nature of TC-mesocyclone circulations. Both radar observations and numerical model results show that these circulations typically extend aloft to an average height of only 3.5 km. Due to the overshooting beam, a circulation of this depth would be detected within a single elevation slice (0.5°) out to 160 km. For detection within two vertically contiguous slices (0.5° and 1.5°), a further restriction to near 100 km would occur.

c. Mesocyclone (M) algorithm detection versus the manual recognition technique

The current WSR-88D M algorithm employs an automatic two-dimensional pattern recognition scheme (Hennington and Burgess 1981). The algorithm searches for counterclockwise circulations at each elevation angle that meet sufficient shear thresholds. It then attempts to vertically correlate ''recognized'' circulations within the same storm through contiguous elevation slices. If any vertically correlated circulations meet predetermined symmetry thresholds, the feature is identified as a mesocyclone. Absence of vertical continuity and/or lack of symmetry results in a designation of a ''shear'' feature. The skill of the algorithm in identifying many mesocyclones is limited by the need for rotation within two vertically linked elevation slices rather than through a specific depth, by adaptable parameter settings ''defaulted'' for average dimension supercells, and by the inability to account for aspect ratio sampling limitations.

Given these limitations, a manual detection technique was developed (OSF 1995) but, again, based largely upon the characteristics of typical Great Plains supercells. Although not exclusive, suggested guidelines for a manual mesocyclone detection include 1) a core diameter less than 9.5 km exhibiting a signature more rotational in nature than divergent; 2) extension of the rotational signature through a vertical depth greater than 3.5 km; and 3) existence of the previous conditions for at least two volume scans (10–12 min). To account for the degradation of measured rotational velocities at increasing range, a constant diameter (6.5 km) mesocyclone nomogram was empirically developed by the WSR-88D Operational Support Facility (OSF) and the Norman, Oklahoma, National Weather Service Office (NWSO) using data collected from

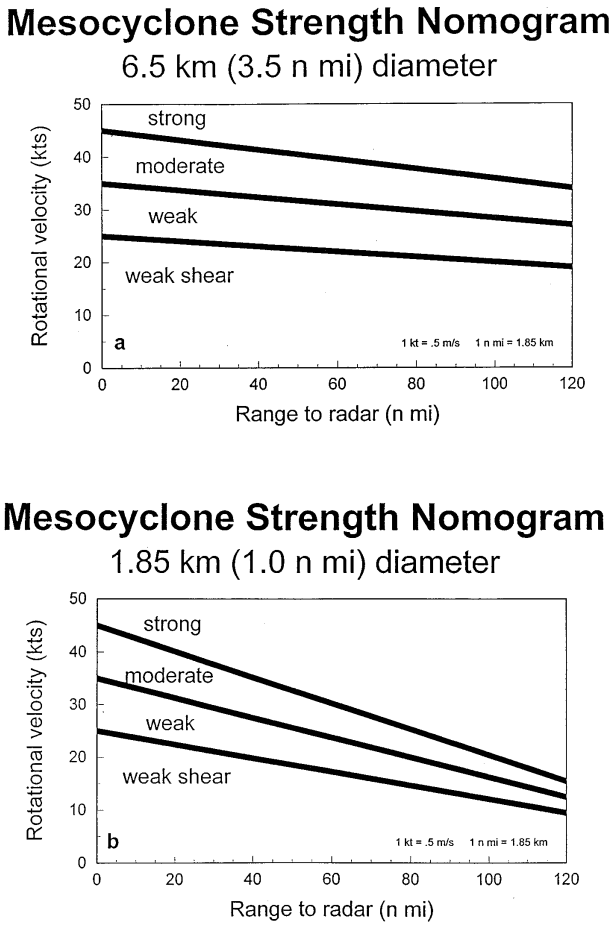

FIG. 2. Operational Support Facility (OSF) mesocyclone strength nomograms (rotational velocity vs range from radar) assuming (a) a typical diameter for Great Plains mesocyclones of 6.5 km or 3.5 n mi (from Andra 1994) and (b) a diameter of 1.85 km or 1.0 n mi, similar to that observed within tropical cyclone rainband mesocyclones. The mesocyclone strength categories were empirically derived from data gathered in the southern Great Plains to better define the relative intensity of circulations.

Great Plains supercells (Fig. 2a). Assuming fulfillment of conditions 1–3 above, a tornado warning is *suggested* when a storm contains a strong mesocyclone or contains a minimal or moderate mesocyclone (Fig. 2a) and other parameters suggest a tornado threat (OSF 1995). Furthermore, the guidelines state that some tornadoes, typically weak and short lived, may occur in the absence of a detectable mesocyclone and that low-topped convection (i.e., tropical) may require a lessening of the 3.5-km circulation depth criteria.

While the manual detection method has many caveats, it does exploit the WSR-88D's sampling skills and complement algorithm assessment to improve the overall probability of detection in real time. With reduced physical dimensions of circulation however, the probability of detection also decreases by either manual or algorithm identification methods. When attempting to assess the strength of detected TC mesocyclones,

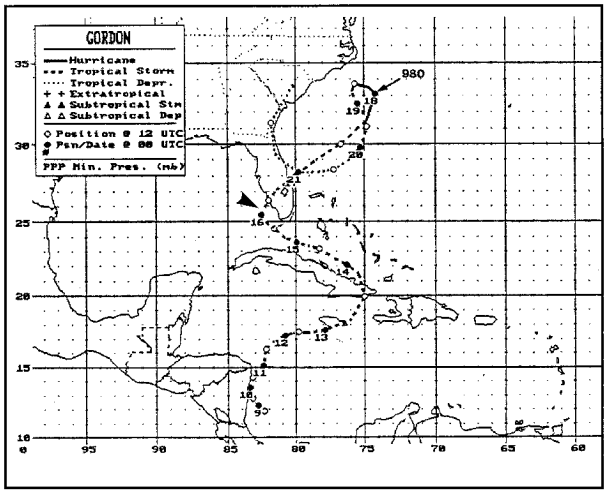

FIG. 3. Best track positions of Tropical Cyclone Gordon. The arrow indicates the approximate position of Gordon during the time of the tornadoes across east-central Florida.

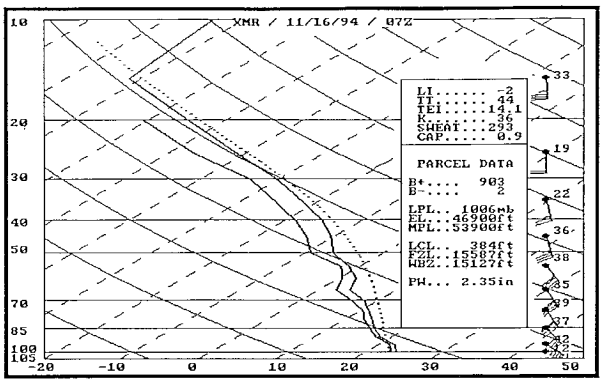

FIG. 4. Thermodynamic sounding from Cape Canaveral AFB, FL, at 0700 UTC 16 November 1994 indicative of the deep tropical moisture. The solid lines represent temperature and dewpoint profiles (°C), and the dotted line indicates an adiabatic displacement of a parcel lifted from the surface. Wind direction and speed (kt) are plotted at selected levels.

the likelihood for smaller dimensions must be considered, especially with increasing range from the radar site. This would negate a strict adherence to the aforementioned OSF guidelines. The authors suggest using an adjusted nomogram for a core diameter of 1.85 km (1.0 n mi; Fig. 2b) rather than the more standard 6.5-km nomogram (Fig. 2a) as an additional method of manual compensation. The steeper slopes of the threshold curves for small diameter rotations (Fig. 2b) represent the more impacting effects of radar-sampling limitations with respect to range. Both nomograms are used in section 4 when assessing relative mesocyclone strengths.

3. Synoptic overview of Tropical Cyclone Gordon

a. Tropical cyclone summary

After initial classification as a tropical depression on 8 November 1994 near the coast of Nicaragua, the system followed a slow, erratic path across the western Caribbean Sea and the eastern Gulf of Mexico while slowly strengthening to moderate tropical storm intensity (Fig. 3). Tropical Storm Gordon made landfall along the southwest Florida coast on 16 November with maximum sustained winds of 22.5 m s^{-1} and a central pressure of 995 hPa. For a complete discussion of TC Gordon, see Avila and Rappaport (1996).

When the TC center reached a position between Key West and Sarasota on 15 November (Fig. 3), several tornadoes occurred across east-central and southeast portions of the Florida peninsula. Of the six confirmed tornadoes that occurred between 2353 UTC 15 November and 0900 UTC 16 November, two were within range of the Melbourne WSR-88D and will be discussed in section 4. These two tornadoes occurred far from the TC center and in the favored right-front quadrant of circulation at an azimuth/range of 36°/340 km and 21°/330 km.

b. Thermodynamic quantities and vertical wind profile

At both 1600 UTC 15 November (not shown) and 0700 UTC 16 November (Fig. 4), thermodynamic soundings from Cape Canaveral (XMR; 56 km north of KMLB) revealed deep moisture and rather limited instability, with CAPE (B+) values of 274 and 903 J kg^{-1}, respectively, assuming lifting of the surface parcel. Conditional instability was generally restricted to below 600 hPa, with a stable layer aloft.

A significant transformation occurred within the vertical wind profile over east-central Florida during 15–16 November as convergent rainbands moved across the region. The evolution of the deep layer wind field is shown in Fig. 5 with bihourly vertical wind profiles produced using winds aloft from KMLB WSR-88D VAD wind profiles (VWPs) and surface winds observed at the adjacent Melbourne International Airport (MLB). The strong unidirectional, easterly flow that had prevailed early on 15 November veered to southeast between 2000 UTC 15 November and 0100 UTC 16 November at and above 0.9 km. At the same time, wind speeds strengthened, reaching 25 m s^{-1} between 0.6 and 1.5 km. These changes resulted in a steady trend of increasing 0–3-km SRH (Fig. 5). The SRH values were computed from hodographs constructed on the SHARP workstation (Hart and Korotky 1991) using the wind profiles shown in Fig. 5 and actual storm motions as determined by radar for the most intense rainband cell within 140 km of KMLB. The 1600 UTC hodograph revealed a rather meager SRH of only 21 m^2 s^{-2} (Fig. 6a); however, this value increased significantly to 296 m^2 s^{-2} only 8 h later as evidenced from the 0000 UTC hodograph (Fig. 6b), indicating a high

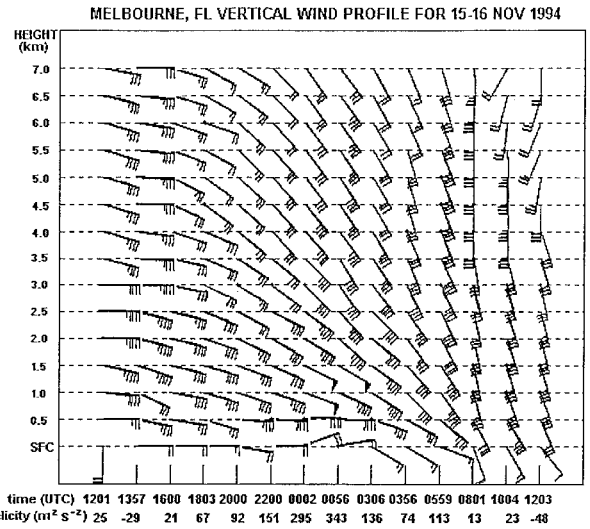

FIG. 5. Vertical wind profile (time vs height cross section) between 1200 UTC 15 November 1994 and 1200 UTC 16 November 1994 constructed using winds aloft from the Melbourne WSR-88D VAD Wind Profile and surface winds from Melbourne International Airport. Winds are plotted using the standard model, with one short barb equal to 2.5 m s^{-1} (5 kt) and a long barb equal to 5 m s^{-1} (10 kt). Storm-relative helicity (SRH) values based upon the individual profiles are shown below each plot. Storm motion vectors were determined by radar for the rainband cell with the highest reflectivity within 140 km of KMLB.

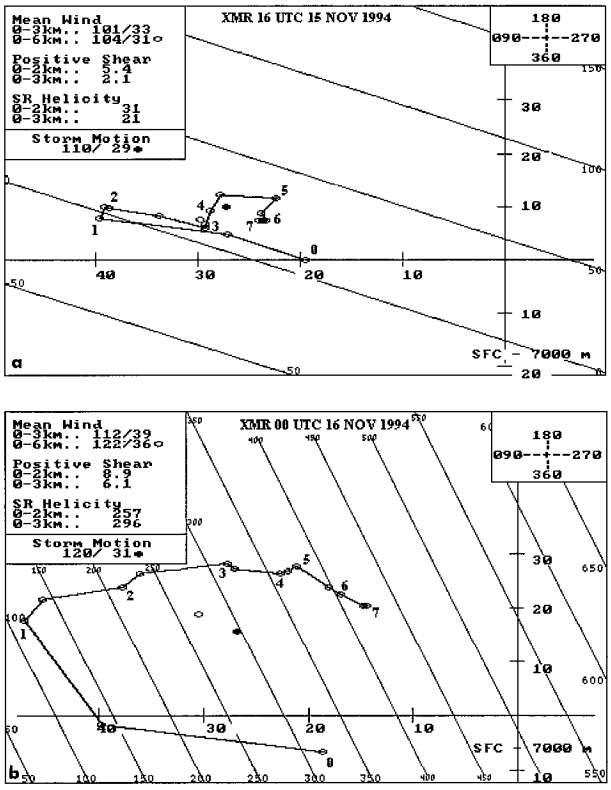

FIG. 6. (a) Hodograph produced using winds aloft from the Melbourne WSR-88D VAD Wind Profile and the surface wind from Melbourne International Airport at 1600 UTC 15 November 1994. Winds are plotted every 0.5 km above ground level (AGL) from the surface to 7 km and labeled every 1 km. The skewed lines represent contours of constant helicity. The table inset lists average wind (kt), shear (10^{-3}), and helicity (m^2 s^{-2}) parameters. Storm motion was determined manually from radar for the highest reflectivity rainband cell within 140 km of KMLB. (b) Same as a except for 0000 UTC 16 November 1994.

potential for rotating storms. Helicity peaked at 343 m^2 s^{-2} at 0056 UTC (not shown), then fell substantially and remained below 25 m^2 s^{-2} from 0800 UTC onward as the favorable shear lifted north of MLB. The northward advection of the helicity was evident from XMR raobs as computed SRH values increased from 80 m^2s^{-2} at 0000 UTC to 175 m^2s^{-2} at 0700 UTC (not shown).

c. Rainband features

Throughout 15–16 November, several broken areas of rainfall on the eastern periphery of Gordon's circulation rotated outward far from the center and became detached from the main convective banding features upon reaching east-central Florida. More importantly, several rainbands developed in situ over the nearshore coastal waters and the immediate east coast and spiraled north and northwest across the adjacent land areas (Figs. 7a and 7b). Initial analyses from the 0000 UTC 16 November Nested Grid Model (not shown) indicated an area of strong low-level convergence and upward vertical motion coincident with the formation region of these rainbands.

Five circulations embedded within the rainbands were classified as persistent in both duration and depth, lasting 1 h or more and identifiable within at least two consecutive elevation angles. Two of these features possessed mesocyclonic signatures while moving over the east-central Florida peninsula and will be referred to below as the Barefoot Bay and Iron Bend mesocyclones. Several of the remaining circulations also likely produced severe weather as at least two large waterspouts were observed offshore; however, these features weakened prior to reaching the peninsula.

4. Radar analysis of mesocyclones associated with TC Gordon

a. Barefoot Bay mesocyclone

1) REFLECTIVITY OBSERVATIONS

Initiation of the feature designated as the Barefoot Bay mesocyclone can be traced back to 2215 UTC 15 November when several small, high reflectivity cells (>50 dBZ) began to develop 130 km southeast of MLB, near the eastern portion of a persistent rainband. Beginning with the 2255 UTC volume scan, the updraft within a cell located 80 km southeast of MLB strengthened as evidenced by increasing reflectivity values aloft. Table 1 details the temporal trend of radar parameters

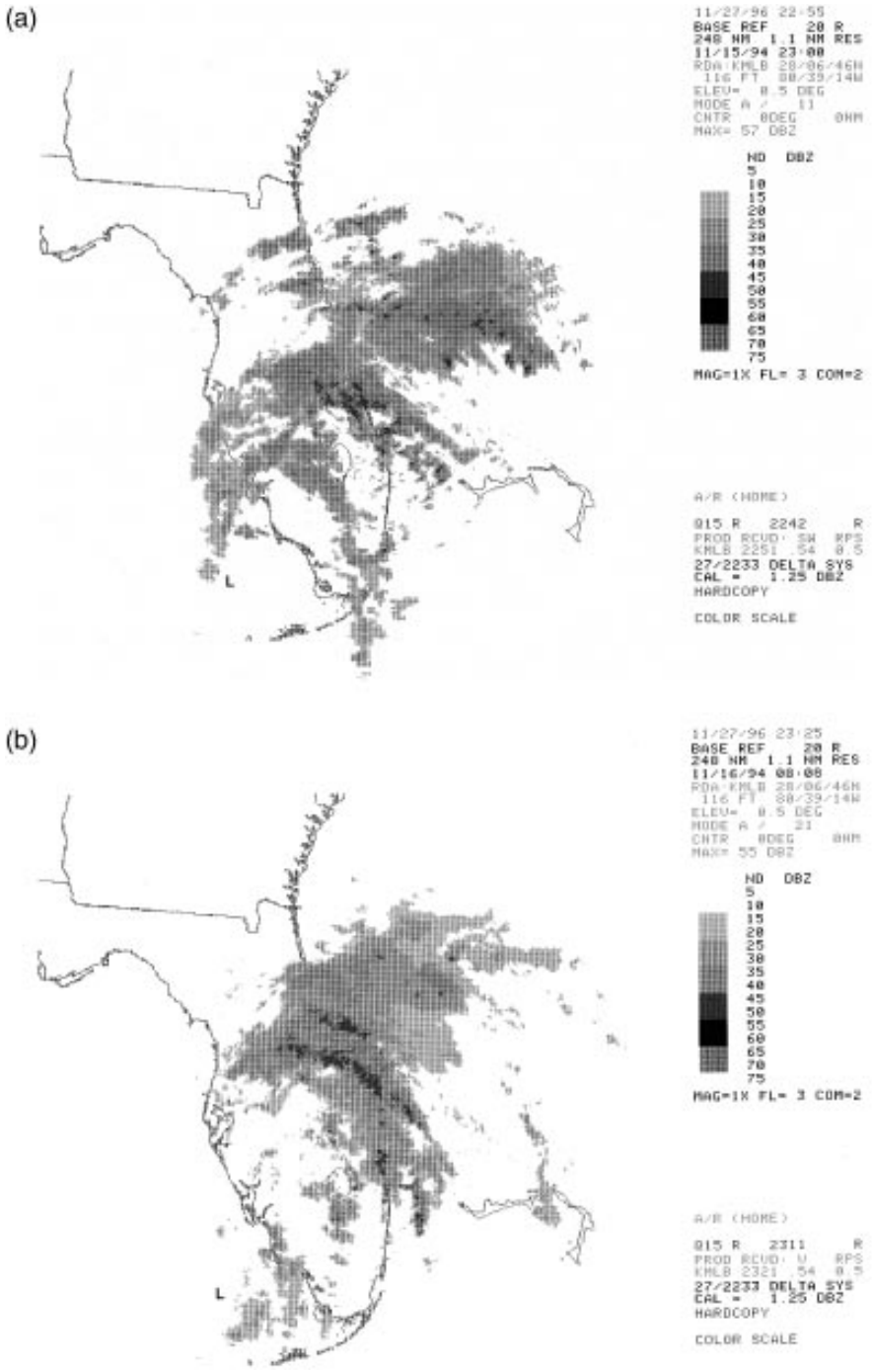

FIG. 7. Large-scale view of TC Gordon's rainbands from the Melbourne WSR-88D 0.5° base reflectivity products at (a) 2300 UTC 15 November 1994 and (b) 0808 UTC 16 November 1994. The letter ''L'' signifies the location of Gordon's center near the time of the radar product.

associated with this cell. During the next 20 min, a core of 55–59 dB*Z* extended upward to the 2.4° elevation (3 km) and an inflow notch became apparent at 2.0 and 3.0 km as the cell continued to move northwest at 15 m s^{-1} (Fig. 8). A transformation then occurred between 2320 and 2335 UTC as moderate to strong echoes (>40 dB*Z*) immediately west of the cell weakened, allowing the cell of interest to become distinct and relatively isolated. Also during this time period, the inflow notch became prominent throughout the lower four elevation angles (0.8–3.7 km), while the reflectivity maxima aloft became displaced 1–2 km northeast of the low-level

TABLE 1. Temporal trend of parameters associated with the Barefoot Bay mesocyclone during TC Gordon, as viewed by the Melbourne, FL, WSR-88D. Tornado time indicated by the arrow.

Time (UTC)	Rng. (n mi)	Echo top (kft)	VIL (kg m^{-2})	Max Refl. (dBZ)	1.5° Hgt. (kft)	1.5° V_R (kt)	1.5° Dia. (n mi)	1.5° Shr. (s^{-1})	0.5° Hgt. (kft)	0.5° V_R (kt)	0.5° Dia. (n mi)	0.5° Shr. (s^{-1})	0.5° SW (kt)
2255	44	45–49	15–19	55–59	8.5	—	—	—	3.9	19	1.8	.006	n/a
2300	41	40–44	15–19	55–59	7.7	25	1.6	.009	3.5	22	1.6	.008	n/a
2305	37	35–39	15–19	55–59	7.0	26	3.0	.005	3.1	21	1.3	.009	12–15
2310	36	35–39	15–19	55–59	6.7	27	0.5	.030	2.9	30	1.7	.010	16–19
2315	33	30–34	15–19	55–59	6.2	30	0.8	.021	2.7	25	0.8	.018	16–19
2320	31	25–29	15–19	55–59	5.6	25	0.7	.020	2.4	26	2.0	.008	16–19
2325	28	35–39	15–19	55–59	5.2	30	2.2	.008	2.2	31	0.8	.022	n/a
2330	26	35–39	15–19	55–59	4.7	25	2.4	.006	2.0	21	0.7	.017	12–15
2335	23	35–39	15–19	60–64	4.3	26	3.5	.005	1.7	16	1.0	.009	16–19
2340	21	35–39	10–15	55–59	3.8	21	0.9	.013	1.6	16	0.7	.013	12–15
2345	19	30–34	15–19	55–59	3.3	25	1.1	.013	1.4	25	1.2	.012	12–15
> 2350	17	30–34	15–19	55–59	2.9	26	1.2	.012	1.2	30	1.1	.016	16–19
2356	14	30–34	15–19	55–59	2.6	21	0.9	.013	1.0	25	1.0	.014	12–15
0007	11	30–34	20–24	55–59	2.0	17	1.0	.011	0.8	17	1.1	.009	n/a
0012	12	30–34	20–24	50–54	2.2	—	—	—	0.8	—	—	—	n/a

Rng. = range from radar site to the cell. Hgt. = height of the radar beam at the given range in thousands of feet (kft). V_R = rotational velocity $[(|V_{(max^{in})}| + V_{(max^{out})})/2]$, where V represents max SRM velocity. Dia. = mesocyclone diameter (distance across the max_{in} and max_{out} velocity couplet). Shr. = mesocyclone shear ($2V_R$/Dia). SW = spectrum width in knots (k+).

core. By 2325 UTC, the cell reached a position 52 km southeast of MLB and the reflectivity gradient tightened significantly along the south and west periphery of the echo. Within the next 10–15 min the cell approached the coast and peaked in reflectivity as a small area of 60–64 dB*Z* was noted at a height of 2 km and a small reflectivity appendage became visible at the lowest elevation angle (0.5 km). The cell reached the beach at 2340 UTC with cyclonic (hooklike) curvature apparent within the low-level 35–55 dB*Z* reflectivity pattern. The small hook feature remained identifiable at heights of 0.5 and 1.5 km as the cell crossed the narrow intracoastal island and waterway, and reached the mainland at 2345 UTC. By the next volume scan (2350 UTC), upon reaching the community of Barefoot Bay, the hook pattern became much less apparent with only a hint of curvature at the 1-km level. Cell organization continued to decrease during the next 10–20 min, and by 0007 UTC 16 November, the hook and notch features were no longer discernable.

2) VELOCITY OBSERVATIONS

Several small, shallow, short-lived, cyclonic circulations were observed between 2200 and 2250 UTC 15 November along the interface between the south side of the aforementioned rainband and the adjacent rain-free region but were not collocated with the high-reflectivity cells identified in the previous section. At 2255 UTC however, indications of a storm-scale circulation were initially observed, coincident with the onset of the reflectivity core growth of the Barefoot Bay cell (see Table 1). Associated weak cyclonic shear was first observed within the 0.5° (1.2 km) storm-relative velocity (SRM) product, then gradually became detectable as far aloft as 3.8 km by 2315 UTC (Fig. 8). During the next 25 min, as the cell moved from 61 to 37 km southeast of KMLB, detected rotational velocities throughout the 0.5–3.0-km layer were in the weak shear to weak mesocyclone categories (7.5–15 m s^{-1}; Fig. 2b). Pronounced rotational changes occurred between 2340 and 2350 UTC as the cell moved from the Atlantic, across the intracoastal island and waterway, and reached the mainland. Rotational velocities increased rapidly throughout each of the lower four elevation angles (0.5–2.5 km), approaching the moderate mesocyclone category of 13–16 m s^{-1}. During this period, the diameter of the detected circulation generally decreased aloft, averaging near 2 km at each level, while the diameter remained nearly constant or increased slightly within the 0.5° slice. Given the observed increase in rotational velocity within the vertical column, combined with the decrease of circulation diameter aloft, detected shear values averaged over the four lowest elevation slices increased steadily from .009 s^{-1} at 2330 UTC to .016 s^{-1} by 2350 UTC.

A poststorm damage survey indicated that the mesocyclonic cell likely spawned a tornadic waterspout over the intracoastal waterway (Fig. 1) near the time of the maximum shear. Minutes later the tornadic waterspout made landfall along the mainland coast, then moved through the Barefoot Bay mobile home community causing F2 damage and numerous casualties. Although the tornado had lifted by the time of the next volume scan, rotation was still evident at 0.5° but had weakened aloft with only an area of broad shear noted. By 0012 UTC 16 November, evidence of circulation had dissipated at all levels. Throughout the 1-h duration of manual mesocyclone detection (13 volume scans), the M algorithm was triggered on only five scans. The

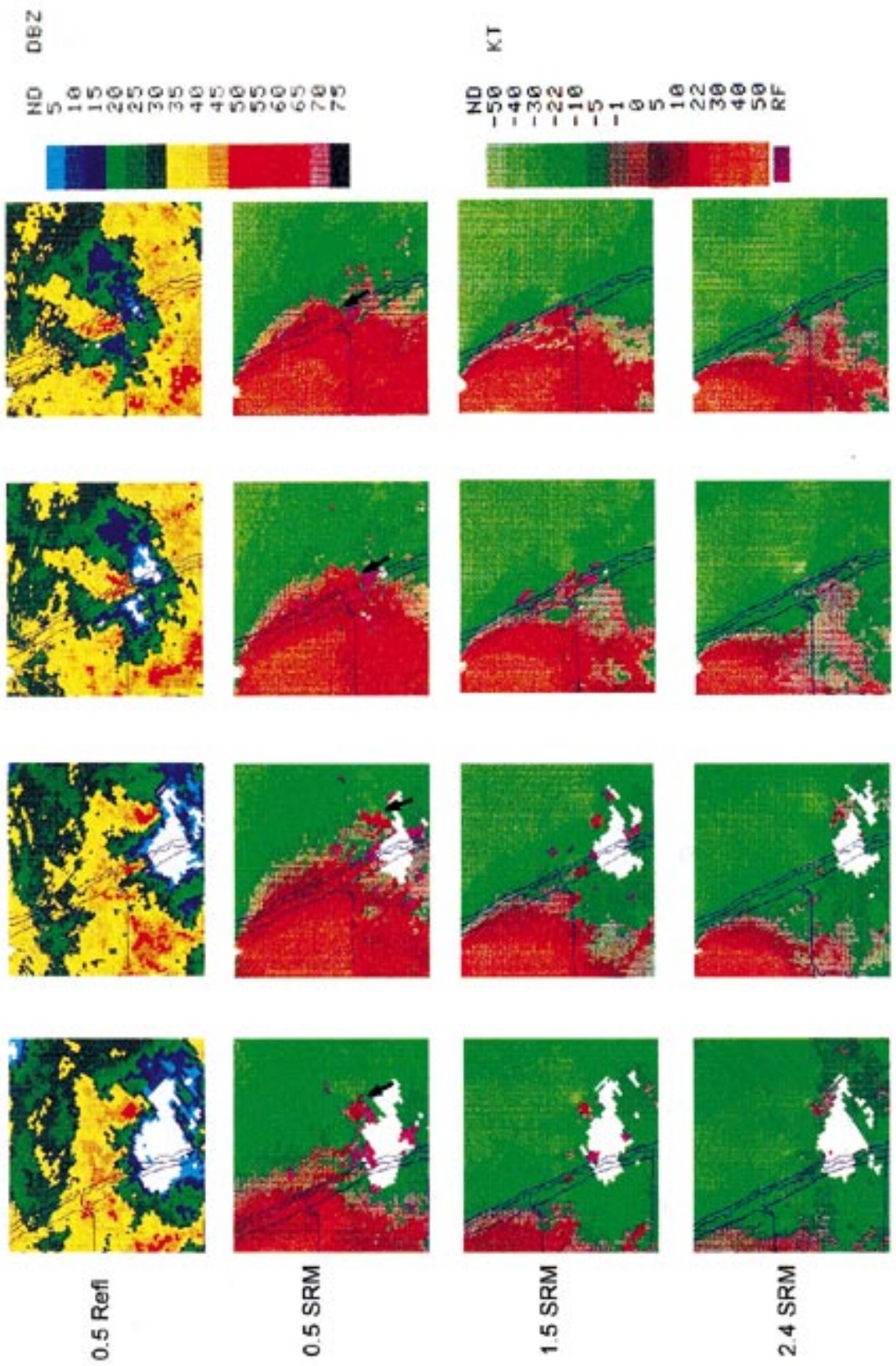

FIG. 8. Selected low-level base reflectivity (Refl) and storm-relative velocity (SRM) products illustrate the evolution of the tornadic Barefoot Bay cell. The images are sized 56 km × 56 km (30 n mi × 30 n mi) and centered on the cell of interest. The Melbourne radar site is located north-northwest of the cell. The reflectivity (dBZ) and velocity (kt) scales are shown near the right margin, and arrows mark the cell of interest.

first three times occurred consecutively between 2300 and 2315 UTC, 5 min after the initial manual detection. The later two times occurred at 2340 and 2345 UTC as the vertical depth of the reflectivity core and rotation increased, 5–10 min prior to tornado occurrence.

3) ANALYSIS

Throughout the life cycle of the Barefoot Bay mesocyclone, VIL values remained very low (15–19 kg m^{-2}), similar to that of the surrounding cells and, therefore, did not highlight the cell of interest. Although the ET product was often difficult to interpret due to numerous small cells in close proximity, the overall trend appears noteworthy. Prior to the cell acquiring rotation, a 14–15-km ET was observed. As rotation became more apparent between 2300 and 2320 UTC, the ET decreased steadily to 7.5–9 km. The ET then increased and remained between 10.5 and 12 km through 2340 UTC, before a more subtle drop to 9–10.5 km occurred as the cell moved onshore. Both trends of decreasing ET corresponded with a time period when rotational velocity and depth were determined to be increasing. Likewise, the M algorithm was only triggered during these periods, indicative of the more restrictive threshold criteria as opposed to manual mesocyclone recognition. Although certainly not definitive, the correlation between ET collapse and mesocyclone strengthening/tornado touchdown often observed during supercell storms (Lemon and Doswell 1979) was noted during this event, although to a much more subtle extent. Examination of SW products indicated an increase of values coincident with the observations of mesocyclone strengthening. Baseline SW values of 6–7.5 m s^{-1} peaked at 8–9.5 m s^{-1} from 2310 to 2320, at 2335, and again at 2350 UTC. When used in concert with the evolution of the reflectivity and SRM signatures, SW trend information offered an additional sign of potential severity.

b. Iron Bend mesocyclone

1) REFLECTIVITY OBSERVATIONS

At 0703 UTC 16 November, a convective band began forming nearly parallel to the central and south Florida coast, and extending northwest to 110 km inland across north Florida. Over the next several hours the band lifted north then rotated cyclonically toward the northwest and eventually southwest back toward Gordon's circulation center. In the area where the band crossed the coastline and just offshore, low-level convergence was maximized and reflectivities were the greatest (50–54 dB*Z*). By 0808 UTC, much of the convection had developed to a fully mature outer rainband, roughly 400 km in length but with a tight radius of curvature of only 90 km (Fig. 7b). Individual cells continued to move through the band toward the northwest at 16 m s^{-1}, indicative of the combined affects of the northward advection of the band segment by the environmental winds and cell propagation. Convection was most vigorous with the northwest-orientated band segment, with low-level reflectivities of 45–54 dB*Z* nearly unbroken across its length.

At 0808 UTC, an apparent weaker-reflectivity notch and higher-reflectivity lobe had formed within convection 60 km northwest of the radar site (Fig. 9). The feature was evident through a 3-km depth with no appreciable tilt or echo overhang. Reflectivities within the lobe were 50–54 dB*Z* with relatively weaker reflectivities of 35–39 dB*Z* within the notch. At 0813 UTC, the notch became coincident with a channel of outbound radial velocities at the lowest level. To its adjacent southwest, the lobe had expanded to a width of 8 km and intensified to reflectivities greater than 55 dB*Z* on its southeast flank, matching spatially with a channel of inbound velocities. Apparent low-level mesocyclogenesis was occurring. Importantly, the notch–lobe features were not remarkably impressive using reflectivity information alone. Table 2 shows the temporal trend of parameters associated with the developing mesocyclone. At 0837 UTC, the entire feature had broadened; however, reflectivities still remained at 50–54 dB*Z*. At 0854 UTC, a section of the band had developed to become quite similar to a northward moving ''bow echo.'' The notch–lobe feature had seemingly become the rotating ''head'' on the west end of the tropical bow. In fact, the trailing sections of the band segment had the general appearance of a line echo wave pattern (LEWP) with two other cyclonically rotating heads (Fig. 10a). The feature was similar to Snell and McCaul's (1993) description of two mesocyclones over Alabama associated with Hurricane Andrew. The west to east orientation of the bow (and LEWP) appeared visually awkward, especially given its northward movement, and was difficult to readily identify in real time due to the reverse orientation compared to typical bow echoes (Przybylinski 1995). The gradient of reflectivity was evenly spaced around the circular-shaped head, however, there was a packing of reflectivities on the north edge of the bow near the apex. The ''bow feature'' exhibited considerable persistence and was subsequently tracked beyond 1000 UTC.

2) VELOCITY OBSERVATIONS

The inspection of storm-relative velocity data proved to be even more revealing, giving greater confidence to reflectivity assessments. Early in the period a series of small, but weak, cyclonic circulations were detected throughout offshore sections of the rainband. By 0750 UTC, the first evidence of rotational organization of the Iron Bend mesocyclone appeared at a height of 2 km as the cell moved onshore and crossed the intracoastal waterway and became positioned 45 km northwest of the radar site. Rotational velocities aloft were 8 m s^{-1}, rep-

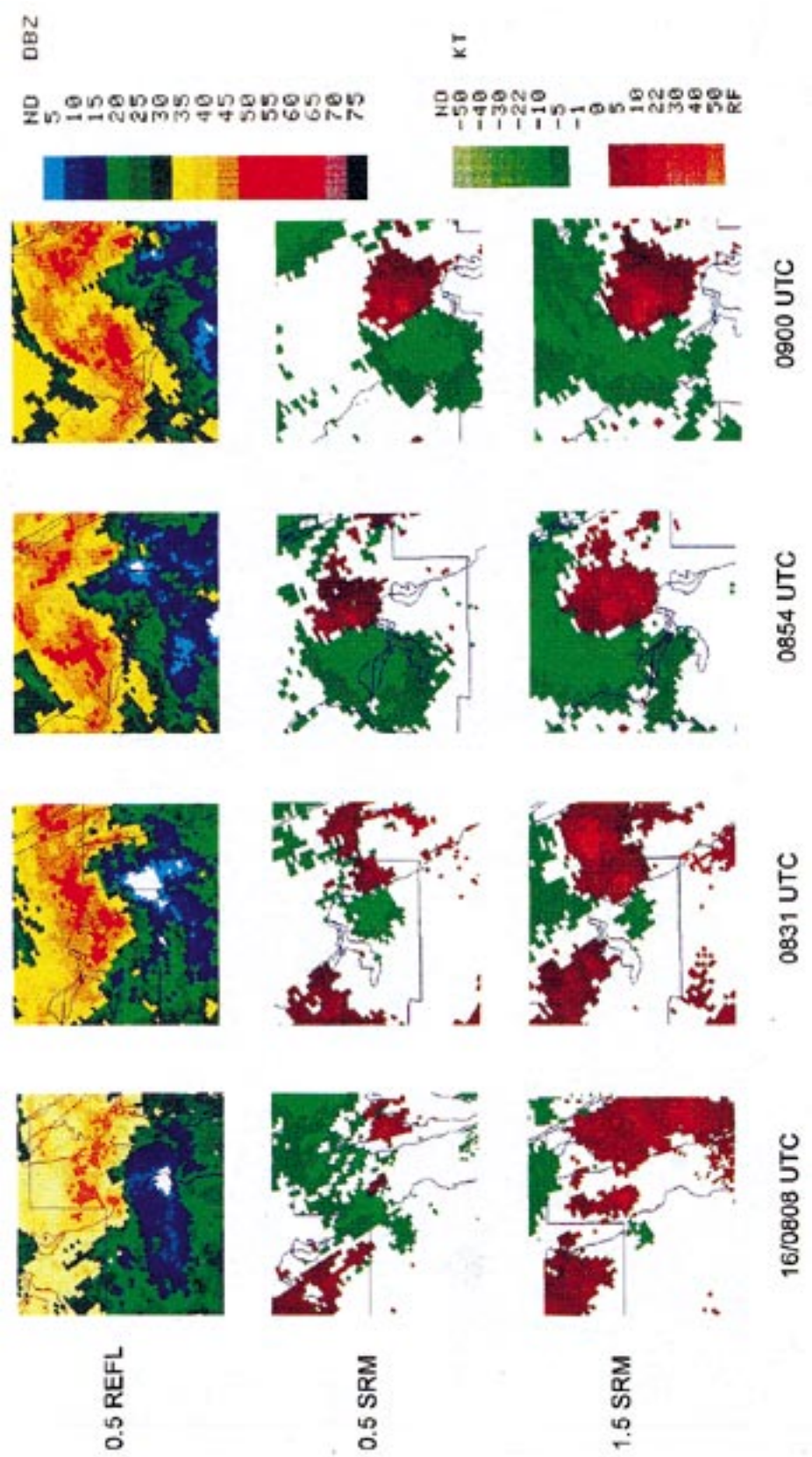

FIG. 9. Same as Fig. 8 except for the Iron Bend cell. The Melbourne radar site is located southeast of the cell.

TABLE 2. Same as Table 1 except for the Iron Bend mesocyclone.

Time (UTC)	Rng. (n mi)	Echo top (kft)	VIL (kg m^{-2})	Max Refl. (dBZ)	1.5° Hgt. (kft)	1.5° V_R (kt)	1.5° Dia. (n mi)	1.5° Shr. (s^{-1})	0.5° Hgt. (kft)	0.5° V_R (kt)	0.5° Dia. (n mi)	0.5° Shr. (s^{-1})	0.5° SW (kt)
0808	32	40–44	20–24	50–54	6.1	21	3.2	.004	2.5	16	0.8	.011	12–15
0813	34	45–49	25–29	55–59	6.6	21	1.8	.007	2.8	21	1.1	.011	12–15
0819	36	40–44	20–24	55–59	7.7	21	1.7	.007	3.0	26	1.0	.015	16–19
0825	40	45–49	20–24	50–54	7.7	21	2.5	.005	3.4	21	1.1	.011	12–15
0831	42	35–39	25–29	55–59	8.4	21	2.0	.006	3.6	26	2.8	.006	12–15
0837	44	35–39	20–24	50–54	8.9	21	3.0	.004	3.9	26	2.0	.008	8–11
0843	46	35–39	15–19	50–54	9.5	21	2.1	.006	4.1	26	3.7	.004	12–15
0848	49	35–39	15–19	50–54	10.0	21	3.0	.004	4.5	26	2.9	.005	16–19
0854	52	35–39	15–19	50–54	10.6	21	4.0	.003	4.8	26	2.2	.007	16–19
> 0900	55	35–39	20–24	50–54	11.3	25	3.8	.004	5.3	35	1.6	.012	16–19
0906	57	30–34	20–24	50–54	12.2	30	5.5	.004	5.5	26	2.0	.008	16–19
0912	59	35–39	20–24	50–54	12.5	21	2.9	.005	5.8	30	3.8	.005	16–19
0918	63	35–39	15–19	50–54	13.2	26	4.6	.004	6.4	25	3.6	.004	16–19
0923	65	35–39	15–19	50–54	13.5	26	3.8	.004	6.7	25	4.0	.004	12–15
0929	64	35–39	15–19	50–54	14.5	25	2.7	.006	6.5	25	4.2	.004	12–15
0935	67	35–39	15–19	50–54	14.7	30	5.3	.004	7.0	16	1.7	.006	8–11
0941	70	35–39	15–19	50–54	15.0	30	5.3	.004	7.4	21	1.8	.007	12–15
0947	71	35–39	15–19	50–54	15.4	25	2.8	.005	7.6	25	2.9	.005	16–19
0953	72	35–39	15–19	45–49	16.1	25	4.8	.003	7.8	25	2.9	.005	12–15
0958	74	35–39	10–14	45–49	16.4	21	3.0	.004	8.0	21	1.6	.008	12–15
1004	76	35–39	10–14	45–49	16.8	25	3.0	.005	8.3	21	1.7	.007	8–11
1010	77	35–39	—	45–49	17.0	21	5.9	.002	8.6	21	1.9	.006	12–15

resenting weak cyclonic shear, with no reflection of discernable circulation at the lowest (0.5°) level. By 0808 UTC, mesocyclogenesis was occurring (Fig. 9) with rotation clearly discernable near an altitude of 3 km and working downward toward the surface. The maximum value of rotation remained aloft around 2 km with a velocity of 11 m s^{-1}. The diameter of the circulation couplet was about 7 km in the midlevels. By 0819 UTC, the low-level circulation intensified to 13 m s^{-1} meeting minimal mesocyclone strength according to the nomogram for a range of 67 km (Fig. 2b). The diameter was slightly over 2 km with a shear value of .015 s^{-1}. The diameter and shear in the midlevels were 4.5 km and .005 s^{-1}, respectively. At 0831 UTC, the mesocyclone was still moving quickly northwest at 18 m s^{-1} away from the radar, and discernable circulation was confined to the two lowest slices of the scan. Minimal mesocyclone strength was observed within the 0.5° slice with weak cyclonic shear at the 1.5° level. Through 0843 UTC, the diameter of the maximum inbound–outbound couplet expanded and contracted between 2.5 and 6 km, impacting the shear trend. By 0848 UTC, the low-level core diameter began significant contraction from a diameter of 6 km, a rotational velocity of 13 m s^{-1}, and a shear of .005 s^{-1} (at a range of 88 km). The first algorithm detection of any type of three-dimensional circulation came with the next scan (0854 UTC) as the core contracted to 4 km and the shear reached 0.007 s^{-1}.

The 0900 UTC volume scan brought the most intense period for the low-level mesocyclone. Rotational velocities soared to 18 m s^{-1} while the core diameter contracted to just over 3 km. Calculations of shear surpassed 0.010 s^{-1} due to the increased rotational velocities combined with the core contraction. At this point, at a range of 100 km, the mesocyclone reached strong intensity (Fig. 2b). During the time period from 0843 to 0900 UTC, the diameter of the core decreased by over one-half and only a single velocity gate separated the maximum wind couplet. Midlevel rotation had also increased to 13 m s^{-1}. The 0900 UTC volume scan also brought the first occurrence of an algorithm-identified mesocyclone. A short-tracked F0 tornado occurred over extreme southern Volusia County (near the Iron Bend area) just prior to 0900 UTC during the period of rapid low-level mesocyclone intensification/contraction. The tornado knocked down numerous trees and caused minor damage to several houses within a very rural area.

3) ANALYSIS

The Iron Bend cell never produced VIL values greater than 25–29 kg m^{-2} (Table 2). Echo tops peaked at 10.5–12 km just prior to the onset of rapid intensification of the mesocyclone, with a reduction noted during the volume scan immediately after tornado touchdown. Spectrum width data did show a well-defined and trackable feature that grew in area and increased in value during the most intense periods of the low-level mesocyclone and was closely correlated to the location of the tornado. The persistence of this mesocyclone was perhaps one of its most impressive characteristics. After producing the brief tornado (Fig. 1), the mesocyclone continued for over an additional hour, well beyond 1000 UTC, without confirmation of additional damage. Interestingly, two other circulations passed through the same area in series with the Iron Bend mesocyclone and associated

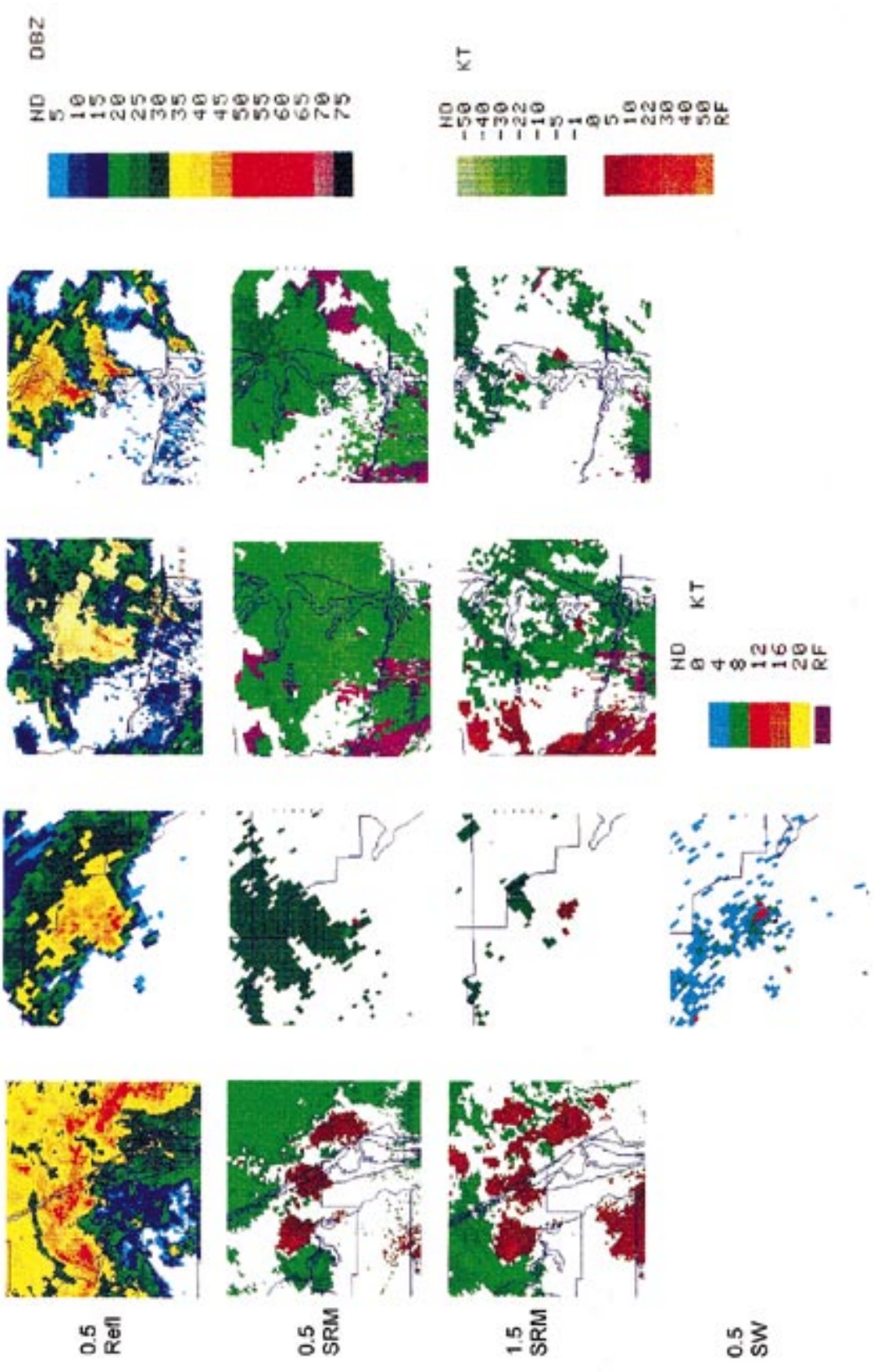

FIG. 10. Selected Refl, SRM, and spectrum width (SW) products illustrate (a) a family of mesocyclones associated with the Iron Bend tropical LEWP at 0900 UTC 16 November 1994, (b) the Polk County mesocyclone at 0305 UTC 5 June 1995, (c) the St. Marys mesocyclone at 0818 UTC 5 June 1995, and (d) a series of mesocyclones downwind from the St. Marys cell at 0957 UTC 5 June 1995. Images in (a) are sized 111 km × 111 km (60 n mi × 60 n mi), and the remainder are 56 km × 56 km (30 n mi × 30 n mi). The WSR-88D sites are located south-southeast of (a) (Melbourne), west of (b) (Tampa Bay), and south of (c) and (d) (Jacksonville).

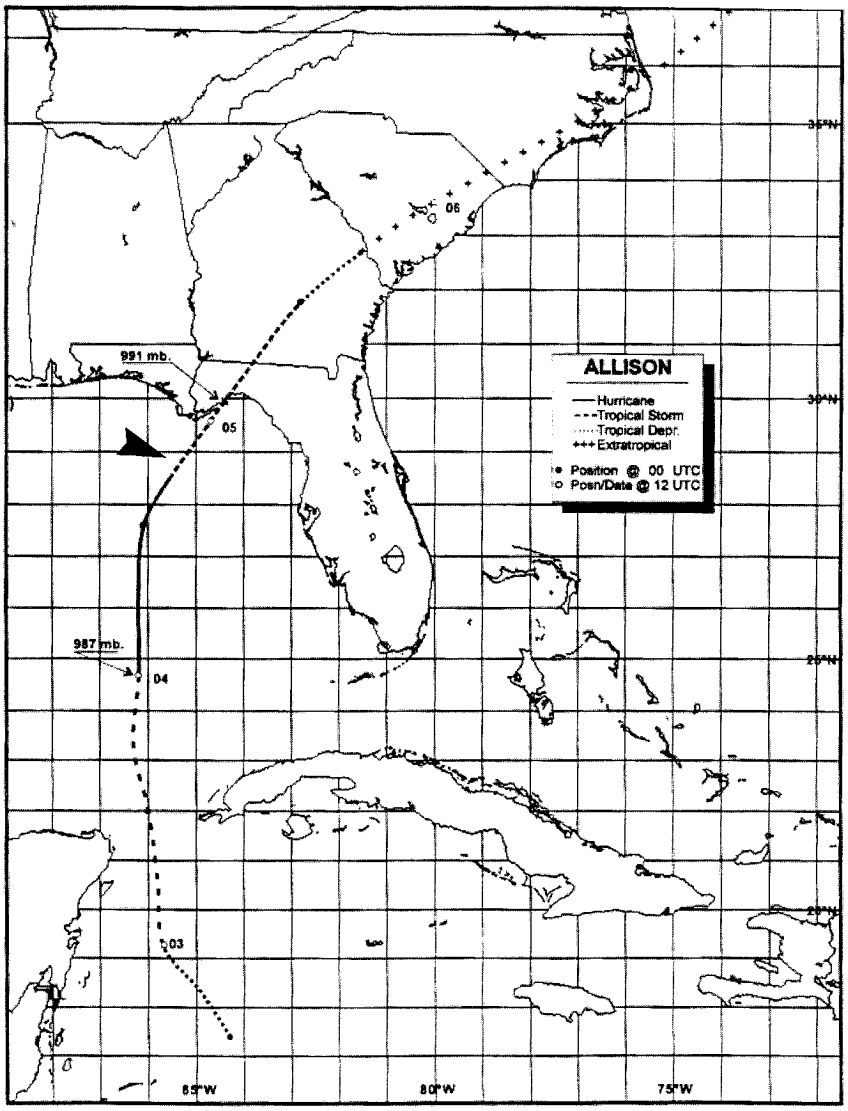

FIG. 11. Best track positions of Hurricane Allison, 3–6 June 1995.

with the head of the bowing subsegment (Fig. 10a) but did not produce damage.

5. Synoptic overview of Tropical Cyclone Allison

a. Tropical cyclone summary

At 0000 UTC 3 June 1995, a tropical disturbance in the northwest Caribbean Sea was upgraded to the first tropical depression of the season. As the system moved north into the eastern Gulf of Mexico, it gradually strengthened and was named Tropical Storm Allison at 1500 UTC 3 June, then reached hurricane status 24 h later. Hurricane Allison made landfall in the ''Big Bend'' area of Florida the morning of 5 June, then continued north-northeast into Georgia and the Carolinas, where it became extratropical (Fig. 11).

During the evening of 4 June, the center of Allison reached a position favorable for tornado development across west-central portions of the peninsula. Although most of the tropical storm force winds remained offshore, an outer convective band did sweep inland from the gulf during this period. Two weak tornadoes formed within the band in association with the same parent cell.

Early on the following day as Allison approached landfall, the favorable tornadic environment shifted northward. Subsequently, eight tornadoes occurred across northeast Florida and southeast Georgia between 0700 and 1300 UTC, several of which were spawned from a single mesocyclone.

b. Thermodynamic quantities and vertical wind profile

Three hours prior to the west-central Florida tornadoes, sounding data from TBW (0000 UTC 5 June)

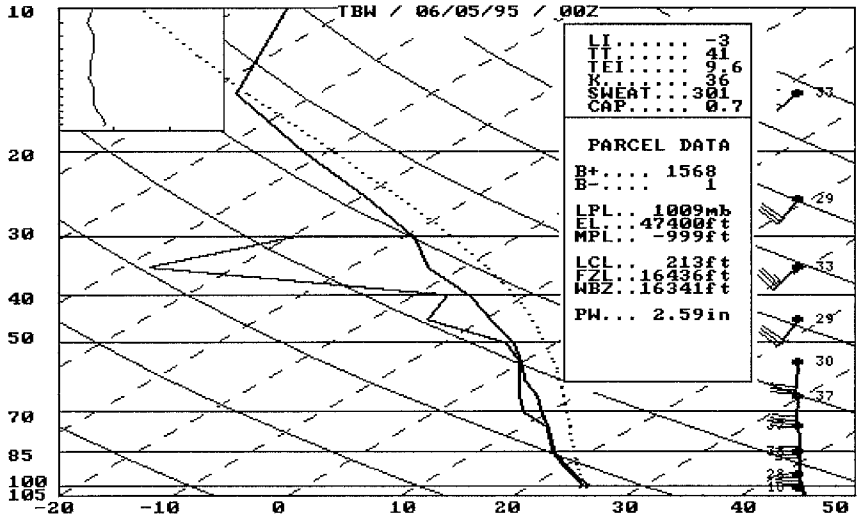

FIG. 12. Same as Fig. 4 except for Tampa Bay, FL, at 0000 UTC 5 June 1995.

indicated the presence of a very moist atmospheric column with a CAPE (B+) slightly above 1500 J kg^{-1} based on lifting a surface parcel and a 0–3-km SRH of nearly 150 m^2 s^{-2} (Figs. 12 and 13) based on observed storm motions. Vertical wind shear changed little throughout the day.

By the following morning (1200 UTC June 5), the JAX sounding revealed an environment similar to that observed at TBW 12 h earlier. During the overnight hours prior to the raob release, the KJAX VWP showed an important evolution of the low-level wind structure as near-surface velocities increased (Fig. 14). The early morning increase of low-level wind shear enhanced vertical turning and produced an environment more favorable for mesocyclone development across northeast Florida and southeast Georgia.

c. Rainband features

As Allison tracked northward through the Gulf of Mexico during the evening hours of 4 June, several convective bands moved northeast across the Florida peninsula. At 2203 UTC, an organized convective band extended from near the center of Allison, east-southeast to the coast west of Tampa Bay, then south along the coast to near Key West (Fig. 15). Shortly thereafter, a radar-detected low-level boundary was observed along and just offshore the southwest Florida coast. Where the boundary and rainband intersected over the coastal waters, a convective cell initiated and began to move northward (Fig. 16).

By 0201 UTC 5 June, the cell of interest had reached the interior of the peninsula and marked the northern

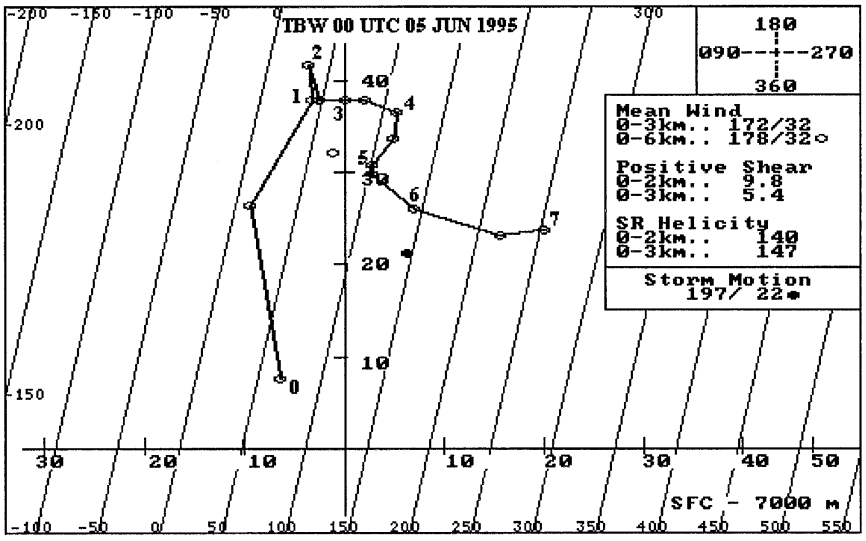

FIG. 13. Same as Fig. 6a except for Tampa Bay, FL, at 0000 UTC 5 June 1995.

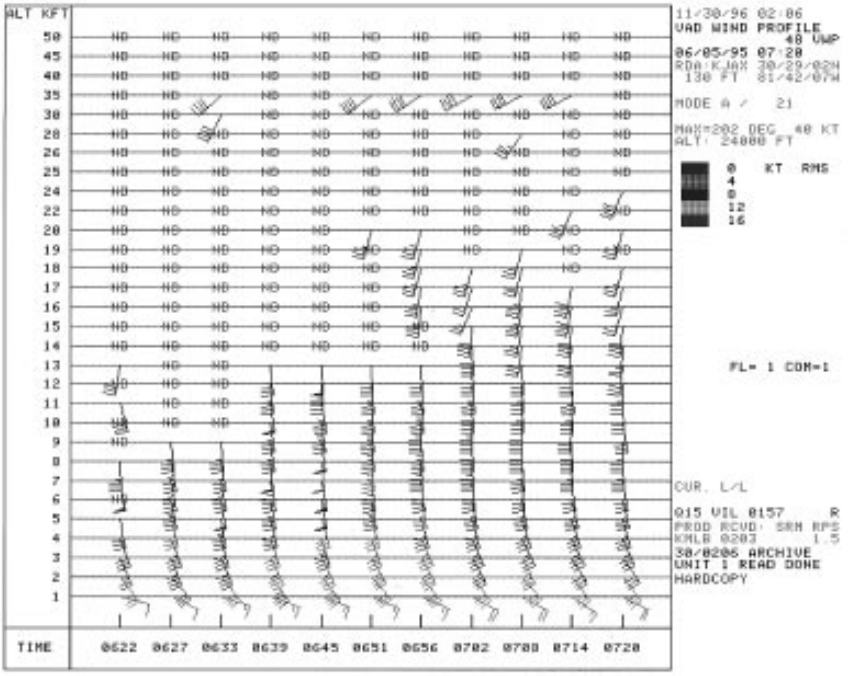

FIG. 14. The Jacksonville velocity azimuth display (VAD) wind profile (VWP) at 0720 UTC 5 June 1995 showing an increase in low-level wind shear between the surface and 5 km (15 kft).

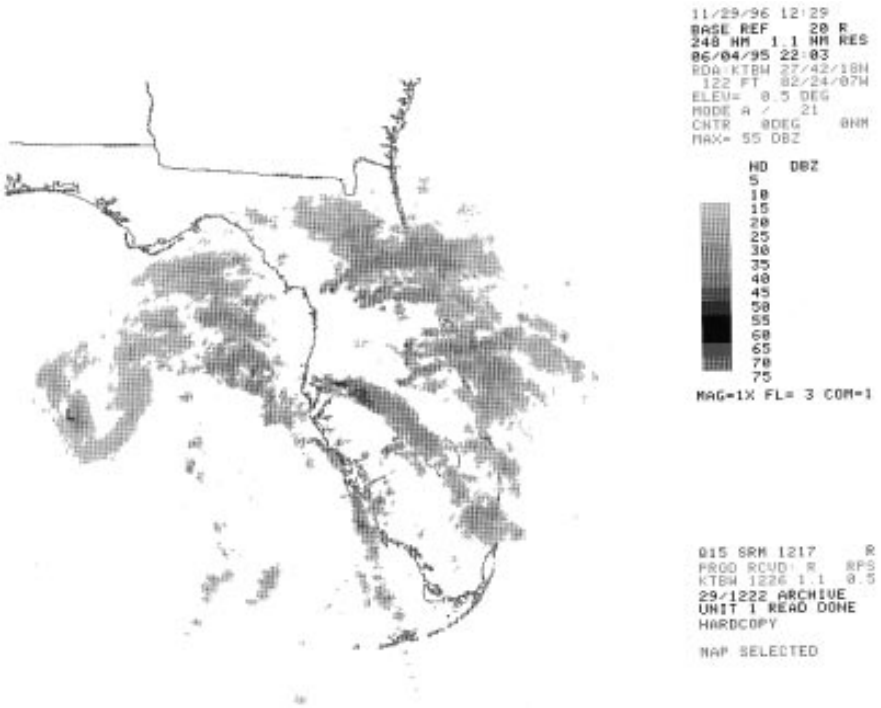

FIG. 15. The 0.5° base reflectivity product from KTBW illustrating the rainband structure at 2203 UTC 4 June 1995. The letter "L" indicates the center of Allison near the time of the radar image.

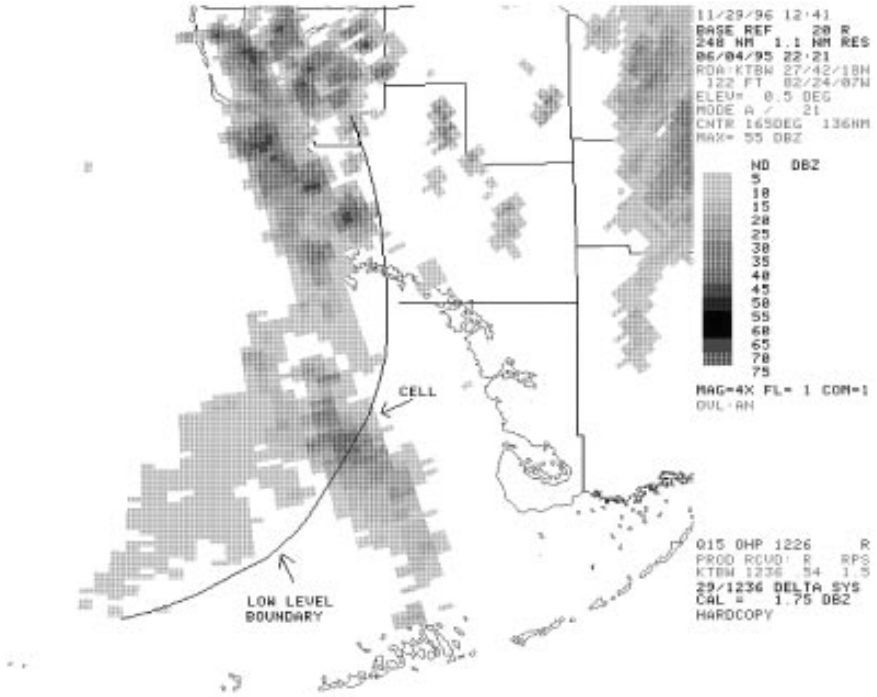

FIG. 16. The 0.5° base reflectivity product for 2221 UTC 4 June 1995. Note the boundary extending offshore from the southwest Florida coast.

end of a newly developed rainband. After producing brief tornadoes 83 km east-northeast and 91-km northeast of KTBW (Fig. 1), the cell collapsed by 0357 UTC. These two tornadoes and their parent cell will be discussed in section 6a.

By 0800 UTC, another rainband had reached north Florida and extended from a large stratiform rain area in the Atlantic Ocean to a second large area of rain well inland, then inward toward the center of Allison (Fig. 17). Although convective activity appeared suppressed near the northeast Florida coastline between the regions of stratiform rain, isolated convective cells were noted.

Throughout the next several hours, numerous mesocyclones developed along a narrow coastal strip within the broad minimum of stratiform and convective rainfall but, nonetheless, along a discernable banding feature. Subsequently, multiple tornado touchdowns occurred in association with the radar-identified mesoscale circulations. Several of these tornadoes were associated with the same parent mesocyclone and will be discussed further in section 6b. The life cycle of these tornadoes and their associated mesocyclone were typical of the remaining events across north Florida and southeast Georgia.

6. Radar analysis of mesocyclones associated with TC Allison

a. Polk County mesocyclone

Examination of the cell of interest prior to the first tornado indicated a persistent maximum reflectivity core between 45 and 49 dBZ through 0230 UTC. Weak cyclonic shear was first observed at the 0.5° and 1.5° elevations around 0213 UTC, with rotational velocities between 6.5 and 9.5 m s^{-1}. Further aloft, rotation was less apparent. Shortly thereafter, a significant change was noted in the diameter of rotation at 1.5° as the very broad circulation of nearly 16 km at 0224 and 0230 UTC lessened to 10 km by 0236 UTC. At the same time an increase of reflectivity to 50–54 dBZ occurred, preceding the tornado touchdown by only minutes. Table 3 capsulizes the temporal trend of parameters observed by radar for this tornadic cell.

By 0242 UTC, near the time of the tornado, maximum reflectivity returned to the 45–49-dBZ range; however, a subtle appendage had become identifiable along with evidence of a bounded weak echo region (BWER). The diameter of the mesocyclone aloft continued to gradually contract, reaching 3.5 km near the time of the tornado. Although diameter changes were not as drastic at 0.5°, a temporary tightening did occur coincident with a rise in rotational velocity, resulting in shear of nearly 0.010 s^{-1} and a weak mesocylone classification according to the strength nomogram (Fig. 2a). The WSR-88D mesocyclone algorithm did not identify the manually detected weak circulation at this time or at any other times. After producing a short path of F0 damage (Fig. 1), the tornado lifted prior to the 0248 UTC volume scan; however, the appendage continued to remain apparent and the reflectivity core again increased to 50–54 dBZ. Although a classic hook signature was never

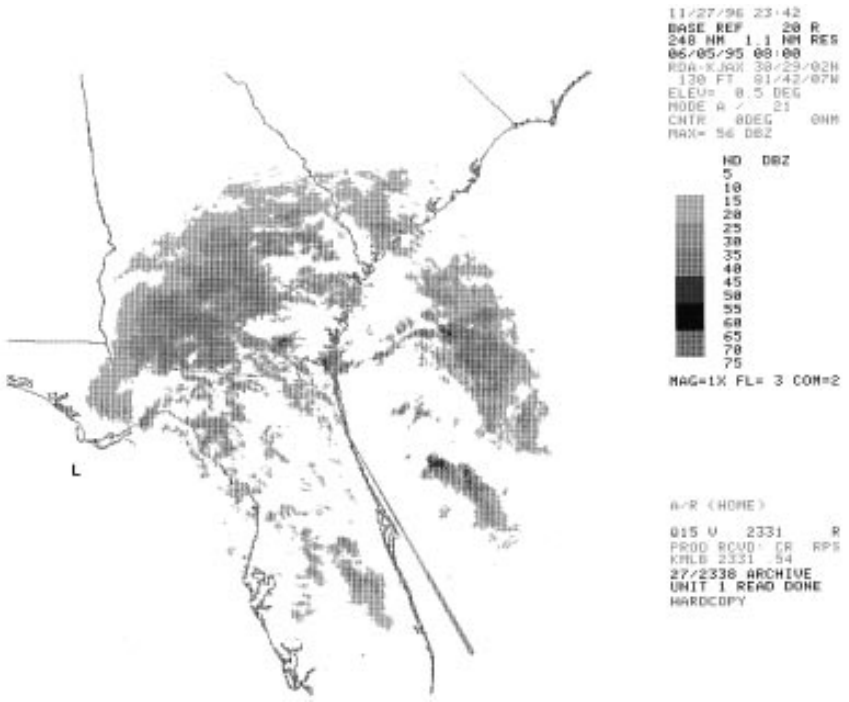

FIG. 17. Same as Fig. 15 except for 0800 UTC 5 June 1995 from KJAX. Note the discontinuous banding from offshore northeast Florida to southwest Georgia.

observed, the appendage and high-reflectivity pattern remained evident during the next few volume scans as the cell continued northward.

The second tornado produced F1 damage along an 11-km-long path between 0310 and 0315 UTC, 30 min after the initial touchdown and 24 km to its north (Fig. 1). As with the first tornado, a manually identified mesocyclone was present but remained weak prior to and during the time of damage, with rotational velocities of 7–11 m s^{-1} at 0.5° and 1.5° (Fig. 10b). The rotational diameter remained near 4 km within the 1.5° slice but decreased to less than 2 km at the lowest level with a corresponding increase of shear to 0.012 s^{-1} just prior to the tornado. After dissipation of the tornado, shear values dropped to 0.008 s^{-1} or less at 0.5° and remained much smaller aloft. As with the first circulation, rotation was apparently too weak and shallow for detection by the mesocyclone algorithm.

Although some cell tilt was observed during the first event, distinction between true tilt and the vertical scan displacement due to the rapid cell movement was difficult to ascertain. The ET product did however help identify the cell as more mature than surrounding echoes with a gradual increase noted from less than 10 km prior to the tornado to nearly 12 km during the touchdown. Echo tops continued to increase after the first event to above 12 km by 0305 UTC, then at about the time of the second tornado the top dropped to 9.0–10.5 km and decreased further to 7.5–9.0 km by 0322 UTC. By the time of the second touchdown, the ET appeared to become displaced far downwind, 11 km from the low-level reflectivity maxima.

VIL values showed little variation throughout both events, ranging between 5 and 14 kg m^{-2} and, therefore, was not a useful product for determining cell severity. These low values were likely due to a combination of cell tilt/rapid motion and the shallow depth of high reflectivity.

The SW product proved to be an interesting and useful tool throughout the duration of the mesocyclone. Values increased steadily from a variance of 4–5.5 m s^{-1} well before the first tornado to between 8 and 9.5 m s^{-1} at 0224 UTC, 20 min prior to touchdown. During the subsequent volume scans, the cell was easily tracked using the persistently high SW signature. Values remained at a maxima of 8–9.5 m s^{-1} and coincided with the time and location of tornado damage, then decreased back to 6–7.5 m s^{-1} after the tornado lifted. Another increasing trend of SW began two volume scans prior to the second tornado, with values again reaching 8–9.5 m s^{-1} by 0259 UTC. During the tornado, SW values remained at a maximum (Fig. 10b) and were again temporally and spatially coincident with the tornado's path. Also as before, SW values decreased when the tornado lifted. This analysis illustrates that using SW in conjunction with other radar products can add confidence during the warning decision process. Use of the SW product may be especially important for ill-sampled storms suffering from ''aspect ratio'' problems, where rotational signatures might be poor to nonexistent.

TABLE 3. Same as Table 1 except for the Polk County mesocyclone associated with Hurricane Allison, as viewed by the Tampa Bay, FL, WSR-88D.

Time (UTC)	Rng. (n mi)	Echo top (kft)	VIL (kg m^{-2})	Max Refl. (dBZ)	1.5° Hgt. (kft)	1.5° V_R (kt)	1.5° Dia. (n mi)	1.5° Shr. (s^{-1})	0.5° Hgt. (kft)	0.5° V_R (kt)	0.5° Dia. (n mi)	0.5° Shr. (s^{-1})	0.5° SW (kt)
0213	42	25–29	10–14	50–54	8.1	15	5.1	.002	3.6	14	2.0	.004	8–11
0219	41	25–29	10–14	45–49	7.9	19	6.2	.002	3.5	18	1.5	.007	12–15
0224	41	30–34	10–14	45–49	7.9	23	8.7	.002	3.5	18	1.5	.007	16–19
0230	42	30–34	10–14	45–49	8.1	19	8.2	.002	3.6	14	1.6	.005	16–19
0236	43	30–34	5–9	50–54	8.3	15	5.3	.002	3.7	13	1.5	.005	16–19
> 0242	43	35–39	10–14	45–49	8.3	15	3.0	.003	3.7	18	1.1	.009	16–19
0248	44	35–39	10–14	50–54	8.5	15	1.8	.005	3.9	23	1.9	.007	12–15
0253	45	35–39	10–14	50–54	8.8	14	1.6	.005	4.0	20	2.8	.004	12–15
0259	46	35–39	10–14	50–54	9.0	14	2.4	.004	4.1	18	2.2	.005	16–19
0305	47	40–44	10–14	50–54	9.2	15	2.2	.004	4.2	23	1.0	.012	16–19
> 0311	48	30–34	5–9	50–54	9.3	15	4.6	.002	4.3	19	1.6	.007	16–19
0317	48	30–34	5–9	50–54	9.3	15	4.9	.002	4.3	14	2.6	.003	12–15
0322	49	25–29	5–9	50–54	9.6	10	3.7	.002	4.5	15	1.1	.008	8–11

b. St. Marys mesocyclone

The St. Marys mesocyclone was responsible for at least two tornadoes. The first official report of a tornado occurred at about 0743 UTC, just south of the Florida–Georgia state line (Fig. 1). The tornado crossed the St. Marys River and lifted without producing much damage. The second tornado occurred from approximately 0812–0825 UTC along a 8-km-long path through St. Marys, Georgia, where F0 damage occurred (Fig. 1). According to the analyzed radar data, there is further evidence of additional tornadic development later in its life. This suggests the cyclic nature of some TC outer rainband mesocyclones.

The St. Marys cell first became identifiable at 0643 UTC, approximately 65 km south-southeast of KJAX. Although the cell did possess intense reflectivity gradients and some weak shear indications early in its life cycle, no other severe weather signatures were initially evident. Table 4 shows the temporal trend of parameters associated with this mesocyclone. As the cell lifted northward, a short-lived BWER became detectable at 0743 UTC, near the time of the reported tornado sighting along the Florida–Georgia line. By 0800 UTC, an inflow notch was observed on the east side of the cell and on the next volume scan a BWER was again seen. The inflow notch remained present at 0812 UTC, about the time of the second tornado touchdown. No discernable relationship was observed between the maximum height of the reflectivity core and the time of tornado touchdown and damage. During the time of the first tornado touchdown at 0743 UTC, only a weak cyclonic shear signature was indicated within SRM products. By 0806 UTC, a narrow-diameter (2.5 km) mesocyclone possessing weak to moderate rotation (15 m s^{-1}; Fig. 2b) was detected. Rotational velocities peaked during the time of the second tornado as a tight couplet was observed, resulting in very high shear values of .029–.033 s^{-1} within the lowest two elevations (Fig. 10c). It is possible that the extreme shear within this particular scan resulted from sampling a portion of the tornado vortex signature rather than the parent mesocyclone. Subsequent scans revealed a trend of gradually increas-

TABLE 4. Same as Table 1 except for the St. Marys mesocyclone associated with Hurricane Allison, as viewed by the Jacksonville, FL, WSR-88D.

Time (UTC)	Rng. (n mi)	Echo top (kft)	VIL (kg m^{-2})	Max Refl. (dBZ)	1.5° Hgt. (kft)	1.5° V_R (kt)	1.5° Dia. (n mi)	1.5° Shr. (s^{-1})	0.5° Hgt. (kft)	0.5° V_R (kt)	0.5° Dia. (n mi)	0.5° Shr. (s^{-1})	0.5° SW (kt)
0726	11	30–34	15–19	50–54	1.9	19	1.0	.011	0.8	22	1.0	.012	n/a
0731	11	30–34	15–19	50–54	2.0	16	1.2	.008	0.8	12	1.4	.007	n/a
0737	10	35–39	15–19	50–54	1.9	14	1.2	.007	0.8	15	1.0	.010	n/a
> 0743	12	30–34	15–19	55–59	2.1	16	1.2	.008	0.8	18	2.4	.005	n/a
0749	12	25–29	15–19	55–59	2.1	16	1.2	.008	0.9	15	1.2	.007	n/a
0755	13	30–34	10–14	55–59	2.4	18	1.2	.009	1.0	15	1.5	.005	n/a
0800	15	25–29	15–19	55–59	2.7	22	1.2	.011	1.1	24	1.4	.010	n/a
0806	17	25–29	15–19	55–59	3.0	22	1.8	.007	1.2	31	1.4	.012	n/a
> 0812	18	30–34	15–19	50–54	3.3	22	1.0	.011	1.3	24	1.5	.009	n/a
> 0818	20	30–34	10–14	50–54	3.6	31	0.6	.029	1.4	36	0.6	.033	n/a
> 0824	22	35–39	10–14	50–54	3.9	21	2.0	.006	1.6	31	1.0	.020	n/a
0829	23	20–24	10–14	50–54	4.2	26	2.6	.006	1.8	25	1.3	.011	n/a
0835	28	20–24	5–9	45–49	5.1	21	3.6	.004	2.2	19	1.6	.007	n/a

ing circulation diameter, to a maximum of nearly 8 km at the 2.4° elevation during the later stage of its life cycle as it moved northward. Just prior to the observed dissipation of the mesocyclone around 1015 UTC, a final brief tornado was reported. Although beyond the scope of this case study, it is important to note that a series of isolated mesocyclones developed downstream from the St. Marys feature between 0800 and 1000 UTC and were also responsible for tornado occurrences (Fig. 10d).

Overall, the St. Marys mesoscale circulation was manually detected for nearly 2 h along a track of about 80 km across Florida and Georgia. Through its life cycle, the mesocyclone remained embedded within a low-level surge of southerly winds. The persistence of the rotational component appeared to have been linked to the large-scale flow feature since the circulation rapidly dissipated once the surge weakened.

7. Operational implications

In order for meteorologists to provide timely weather warnings for TC outer rainband tornadoes, a thorough, yet prompt examination of WSR-88D data is essential. Given the small dimensions of most TC–tornado-producing cells and the often subtleness of their reflectivity signatures as severe indicators, the decision to issue severe weather warnings can prove to be more arduous than during situations involving more traditional mesocyclones/supercells. Furthermore, since TC–outer rainband cells are less likely to produce either large hail or damaging straight-line winds, the effectiveness of issuing severe thunderstorm warnings in lieu of tornado warnings is questionable, even for marginal situations, and is discouraged by the authors. To promote an aggressive radar approach, operators must be able to recognize potential tornadic cells early in their life cycle while compensating for radar sampling limitations. The following sections will address these issues and present an operational approach for identifying potentially tornadic cells within TC outer rainbands.

a. Compensating for WSR-88D sampling limitations

Although traditional severe weather indicators were occasionally observed in reflectivity products during several of the Gordon and Allison tornado events (e.g., inflow notches, pendants, or hooklike echoes), most often the features were more subtle. Even when detected, they were usually at or below cloud base or within 1 km of the surface. Assuming standard atmospheric refraction of the 0.5° elevation (lowest) beam, detection of such features beyond 55 km of the radar site becomes unlikely. Fortunately, mesocyclonic rotation often extended to slightly higher heights. Cyclonic shear, or rotational velocities of weak mesocyclone strength (Figs. 2a and 2b), were observed to a height of nearly 3.5 km within all the studied cases. This height equates to detection distances of approximately 160, 100, and 65 km for the 0.5°, 1.5°, and 2.4° elevation slices, respectively. At ranges where only the beam from one or two elevations intersects a cell below 3.5 km, the vertical continuity threshold for warning decisions should be relaxed since the average updraft itself is only 3.5 km (Weisman and McCaul 1995). A cell possessing weak cyclonic shear or rotation at low or midlevels and high reflectivity relative to surrounding cells should be immediately categorized as suspect, especially if persistence is noted or a history of wind damage exists.

One method of compensating for the WSR-88D's decreased skill in sampling small features at greater distances is to examine a mesocyclone strength nomogram based upon the detected circulation's core diameter. For example, at a range of 160 km, the strength of a given mesocyclone with a rotational velocity of 15 m s^{-1} and diameter of 6.5 km would be classified as minimal, while the same feature with a contracted diameter of 1.85 km would be classified as strong (suggestive of a tornado warning).

Beam broadening at increased ranges also increases the potential for sampled inbound/outbound velocities to be unrepresentative. In these circumstances, relatively high SW values (i.e., >7.5 m s^{-1}) may add confidence to the determination of marginally severe cells.

Due to the small, shallow nature of most TC mesocyclones, it is not surprising that the current WSR-88D M algorithm often results in underdetection. It should be noted that reducing the threshold pattern vector adaptable parameter within the M algorithm (to allow for the identification of smaller 2D circulations) did not dramatically improve its performance during the Barefoot Bay mesocyclone–F2 tornado. Therefore, until a more robust mesocyclone algorithm is employed, manual mesocyclone recognition must be stressed.

Additionally, the relatively long periodicity of WSR-88D data refresh (5–6 min) could be detrimental when attempting to assess parameter trends within cells capable of producing tornadoes of similar or lesser duration. One way to shorten the period for data refresh in the lower elevations would be to manually restart the volume scan once the beam reaches a sufficient elevation (e.g., 4.3°). Although this procedure would preclude algorithm processing of volumetric derived products, a sporadic one-time reexamination of the lower elevations may outweigh the usefulness of such products during fast-breaking events.

b. Operational recommendations

1) ENVIRONMENTAL ASSESSMENT

As TC outer rainbands begin to affect a particular area, frequent assessment of the local environment becomes necessary to determine whether the profile of vertical shear is becoming more favorable for tornadoes. The most useful tool for this purpose is the WSR-88D VWP product. Interactive workstations (i.e., SHARP) can also be utilized to assess specific changes to SRH. In addition, greater thermodynamic destabilization through the intrusion of dry

air aloft or diabatic warming of the near-surface layer can further increase updraft speeds and the potential for tornadic mesocyclones (Vescio et al. 1995). This is more likely to occur during postlandfall ''remnant'' cases, as was observed over the mid-Atlantic region in association with TC Beryl (Vescio et al. 1995) or with extratropical hybrid cases, rather than during prelandfall events.

2) RAINBAND ASSESSMENT

Climatologically, low-level shear is maximized within the northeast quadrant of tropical cyclone circulations. Within this region, local enhancements to shear and vorticity occur along convergent boundaries. As a result, organized rainbands inherently possess a higher degree of concentrated vorticity than less organized adjacent regions. Additionally, the smaller radius of curvature of some rainbands may further act to locally concentrate convergence and vorticity. In order to exploit the available vorticity for mesocyclogenesis (and perhaps tornadogenesis), improved lift is needed to overcome low buoyancy. Such lift, and subsequent cell intensification, may result from sustained updrafts produced via frictional convergence as rainbands move onshore within highly sheared environments (Powell 1988) and from localized convergence along and near intersecting or merging boundaries. Boundary interactions are more likely to occur with rainbands that rotate outward far from the cyclone center or with TC remnants as opposed to rainbands located within the highly organized structure of the inner bands of a mature tropical cyclone. Both frictional convergence and intersecting boundaries also appear to have been factors during the Gordon and Allison tornadoes.

Operationally, both advecting rainbands and the development of bands in situ necessitate a greater degree of scrutiny than adjacent ill-organized regions of stratiform rain with embedded convection. Observations indicated that small mesocyclonic circulations were generated more often within persistent bandlike features than within transient, less persistent features. Organized bands should be closely evaluated for mesocyclones to develop in series, or in banded families, as was also seen with both Gordon (Fig. 10a) and Allison (Fig. 10d).

3) STORM-SCALE ASSESSMENT

Although maximum reflectivity values associated with tropical tornadic cells may not necessarily be impressive, often they will be greater and more persistent relative to adjacent cells. Likewise, ET, VIL, and SW values may be greater and more persistent. Fundamental to the early recognition of suspect cells is the interrogation of the most intense cells within the rainband, regardless of their actual intensity values. A scan by scan examination of suspect cells should be performed by comparing the evolution of reflectivity and SRM velocity products for trends that favor intensification. Also, when assessing SRM products, the radar operator should be cognizant of the average motion vector that is being subtracted from the radial velocities since an erroneous motion can visually mask rotational signatures. Indications of persistent, organized shear or weak rotation within SRM products should be taken seriously, even in the absence of traditional severe weather reflectivity indicators. Likewise, persistent cells that exhibit relatively high reflectivity (compared to surrounding echoes) and remain isolated should be monitored closely for early indications of circulation.

Postanalyses of the Gordon and Allison radar data indicated a close correlation between the time of tornado touchdown and the time of contraction of the low-level mesocyclone. Preliminary results based upon this limited study show that mesocyclones exhibiting shear values of $0.010\ s^{-1}$ or greater should be considered prime candidates for tornadogenesis. As the shear approaches $0.015\ s^{-1}$, the likelihood of tornado formation appears to increase significantly. Likewise, Grant and Prentice (1996) in a study of 16 nontropical low-topped mesocyclones found the magnitude of maximum shear doubled in a 24-min period prior to tornado time, reaching a peak of $0.015\ s^{-1}$ at the time of touchdown. Given these findings, the prompt issuance of a tornado warning is strongly suggested at times when environmental conditions are favorable for tornadoes and small-diameter mesocyclones with moderate to large shear are detected. Nonetheless, it is imperative that radar operators understand the relationship concerning the variability of both the core diameter and rotational velocity on the shear and how well each can be sampled at varying ranges from the radar. Understanding this relationship also places great importance on operator skill for properly discerning the mesocyclone core (i.e., perceiving the idealized Rankine-combined vortex) for diameter, rotational velocity, and shear assessments.

4) FUTURE REQUIREMENTS

Improved forecasts and warnings of TC outer rainband tornadoes will likely occur as additional radar case studies are examined and model simulations evolve. Incorporated improvements at the local office level have already lead to successful tornado detections and warnings during the tornadic outbreak associated with Tropical Storm Josephine (1996) over central Florida. Base data archival (archive level II) from the WSR-88D during TC events should be given a high priority so that new and improved algorithms can be pursued and adaptable parameter optimization can continue. The use of radar-based trend tables must be expanded and exploited to help identify potentially severe cells from the multitude of cells upon the radar display.

Finally, a new VCP should be developed to allow additional low-level scanning with a faster refresh interval. For example, a VCP with added tilts between the surface and the current 0.5°, 1.5°, and 2.4° tilts would provide valuable vertical information for shallow phenomena. To compensate for the additional slices and reduce the data refresh rate to approximately 3 min, many upper elevation

tilts could be sacrificed. This proposed scan strategy would allow for a better and more frequent assessment of phenomena at lower heights where TC mesocyclones are most likely to be detected and would also likely improve algorithm detection efficiencies. The use of this VCP would presumably be restricted to relatively rare events, but ones of great importance to the entire radar-user community.

8. Summary and conclusions

The study of TC-outer rainband tornadoes must continue until a full understanding of their occurrence is obtained. Although the majority of these tornadoes are weak, cases have supported the occurrence of strong tornadoes. Additionally, their small dimensions make them more difficult to sample using current radar technology and their often short-lived nature makes the timeliness of warnings paramount. Therefore, raising the level of anticipation and skill of radar meteorologists during such situations is critical (Spratt and Nash 1995).

Although the characteristics of Great Plains mesocyclones have been studied for some time, not until recent years has the related class of ''minisupercells'' (Burgess et al. 1995), ''low-topped supercells'' (Grant and Prentice 1996), ''toy supercells,'' or ''shallow supercells'' (Cammarata et al. 1996) stimulated research. Although the shallow TC mesocyclones that occurred during Gordon and Allison possessed characteristics similar to other nontraditional mesocyclones, each feature exhibited unique traits when compared among themselves. One such uniqueness involved the Iron Bend mesocyclone, which appeared to be associated with a rotating vortex on the left flank of an individual bow echo in a series of trailing bows within a tropical LEWP. Radar observations of the Gordon–Allison TC mesocyclones proved them to be more physically compact, having reduced vertical depths and smaller horizontal diameters when compared to traditional mesocyclones. The magnitude of rotational velocity was also less, but with comparable shear. Echo tops peaked at an average of 12–15 km similar to the Danny and Andrew events (McCaul 1987; Weiss and Otsby 1993), with average mesocyclone depths of about 3–3.5 km, vertically consistent with the level where environmental shear began to decrease with height.

During the mature stages, the diameters of the low-level core mesocyclones lessened to approximately 1–2 km. Of the four analyzed mesocyclones, all produced short-lived tornadoes, with the Polk County and St. Marys mesocyclones attaining tornadogenesis more than once. This may add to the evidence that supports the possible cyclic nature (growth/collapse) of some TC mesocyclones similar to that of traditional mesocyclones as suggested by Cammarata et al. (1996).

The most devastating tornado (F2) occurred with the Barefoot Bay mesocyclone as it moved onshore. While sufficient vertical shear was provided by the large-scale circulation of the distant tropical storm, it is possible that abrupt changes in near-surface frictional stress at the coast enhanced mechanical mixing and provided the additional shear (Powell 1982; Zubrick and Belville 1993) necessary for tornado development. The effects of this frictional convergence also may have been maximized due to the perpendicular orientation of the rainband relative to the coastline. The authors speculate that interactions between incipient boundaries and TC outer rainbands may have provided local vorticity and vertical motion enhancements during the Allison mesocyclones as well. Interestingly, additional weak circulations were present during each of the four cases that did not produce tornadoes. Also, no tornadoes occurred during either TC absent of manually identified mesocyclones.

Although traditional severe weather reflectivity signatures were often subtle, in each case the tornado-producing cell was associated with a reflectivity maxima greater than those of surrounding cells. Appendages, hooks, and BWERs were not always apparent, especially for cells at greater ranges. However, the occurrence of such signatures within this environment should add a high degree of confidence to the warning decision.

The use of spectrum width information was valuable for the Iron Bend and Polk County mesocyclones as they moved farther away from the radar sites. High SW was found to be a reasonable way to track suspect cells at greater distances, again adding confidence to the warning process in such circumstances.

To complement reflectivity data, the use of SRM information is critical to timely assessment. The persistence of a given mesocyclone raises its potential as a suspect cell. It was found that mesocyclones with low-level core diameters less than 2 km were particularly suspect. The trend of a mesocyclone's shear proved to be more useful than simply assessing the magnitude of its rotational velocity. A shear value of 0.010 s^{-1} within 2 km of the surface correlated well with tornadogenesis and is suggested as a minimum threshold for categorizing cells having a high potential for tornadogenesis, especially if contraction of the mesocyclone diameter occurs. Of course the shear threshold can also be realized from an increase of rotational velocity within a quasi-steady-state mesocyclone possessing a small diameter.

Given the need for improved radar sampling during TC-tornado environments, the authors challenge the development and implementation of a new scan strategy (volume coverage pattern, VCP) to increase low-level vertical resolution and scan time.

Acknowledgments. The authors appreciate the support from the NWS Southern Region Scientific Services Division during this project. The authors extend their gratitude to Dr. Mark Powell, Andy Nash, Dan Petersen, Bradley Colman, and an anonymous reviewer for their many helpful suggestions. Dave Jacobs is recognized for his contributions to the production of the color graphics, as well as Mike Turner for his data processing assistance. Dave Andra and Bob Lee provided the original mesocyclone nomograms used in Fig. 2a and 2b, respectively.

REFERENCES

Avila, L. A., and E. N. Rappaport, 1996: Atlantic hurricane season of 1994. *Mon. Wea. Rev.,* **124,** 1558–1578.

Black, P. G., and F. D. Marks, 1991: The structure of an eyewall meso-vortex in Hurricane Hugo (1989). Preprints, *15th Conf. on Hurricanes and Tropical Meteorology,* Miami, FL, Amer. Meteor. Soc., 579–582.

Bluestein, H. B., and M. H. Jain, 1985: Formation of mesoscale lines of precipitation: Severe squall lines in Oklahoma during the spring. *J. Atmos. Sci.,* **42,** 1711–1732.

Burgess, D. W., R. J. Donaldson, and P. R. Desrochers, 1993: Tornado detection and warning by radar. *The Tornado: Its Structure, Dynamics, Predictions and Hazards,* C. Church, D. Burgess, C. Doswell, and R. Davies-Jones, Eds., Amer. Geophys. Union, 203–221.

——, R. L. Lee, S. S. Parker, D. F. Floyd, and D. L. Andra, 1995: A study of mini supercells observed by WSR-88D radars. Preprints, *27th Conf. on Radar Meteorology,* Vail, CO, Amer. Meteor. Soc., 4–6.

Cammarata, M., E. W. McCaul, and D. Buechler, 1996: Observations of shallow supercells during a major tornado outbreak spawned by Tropical Storm Beryl. Preprints, *18th Conf. on Severe Local Storms,* San Francisco, CA, Amer. Meteor. Soc., 340–343.

Davies-Jones, R. P., D. Burgess, and M. Foster, 1990: Test of helicity as a tornado forecast parameter. Preprints, *16th Conf. on Severe Local Storms,* Kananaskis Park, AB, Canada, Amer. Meteor. Soc., 588–592.

Fujita, T. T., 1993: Damage survey of Hurricane Andrew in South Florida. NOAA *Storm Data,* **34** (8), 25–29.

——, K. Watanabe, K. Tsuchiya, and M. Shimada, 1972: Typhoon-associated tornadoes in Japan and new evidence of suction vorticies in a tornado near Tokyo. *J. Meteor. Soc. Japan,* **50,** 431–453.

Gentry, R. C., 1983: Genesis of tornadoes associated with hurricanes. *Mon. Wea. Rev.,* **111,** 1793–1805.

Grant, B., and R. Prentice, 1996: Mesocylone characteristics of mini supercell thunderstorms. Preprints, *15th Conf. on Weather Analysis and Forecasting,* Norfolk, VA, Amer. Meteor. Soc., 362–365.

Hagemeyer, B. C., and S. J. Hodanish, 1995: Florida tornado outbreaks associated with tropical cyclones. Preprints, *17th Conf. on Hurricanes and Tropical Meteorology,* Miami, FL, Amer. Meteor. Soc., 312–314.

Hart, J. A., and J. Korotky, 1991: The SHARP workstation version 1.50 user's manual. National Weather Service, NOAA, U.S. Dept. of Commerce, 30 pp. [Available from NOAA, National Weather Service, Eastern Region Headquarters, 630 Johnson Ave., Bohemia, NY 11716-2626.]

Hennington, L. D., and D. W. Burgess, 1981: Automatic recognition of mesocyclones from single Doppler radar data. Preprints, *20th Conf. on Radar Meteorology,* Boston, MA, Amer. Meteor. Soc., 704–706.

Hill, E. L., W. Malkin, and W. A. Schulz Jr., 1966: Tornadoes associated with cyclones of tropical origin–practical features. *J. Appl. Meteor.,* **5,** 745–763.

Klazura, G. E., and D. A. Imy, 1993: A description of the initial set of analysis products available from the NEXRAD WSR-88D system. *Bull. Amer. Meteor. Soc.,* **74,** 1293–1311.

Lemon, L. R., and C. A. Doswell, 1979: Severe thunderstorm evolution and mesocylcone structure as related to tornadogenesis. *Mon. Wea. Rev.,* **107,** 1184–1197.

Marks, F. D., and R. A. Houze, 1984: Airborne doppler radar observations in Hurricane Debby. *Bull. Amer. Meteor. Soc.,* **65,** 569–582.

McCaul, E. W., Jr., 1987: Observations of the Hurricane ''Danny'' tornado outbreak of 16 August 1985. *Mon. Wea. Rev.,* **115,** 1206–1223.

——, 1990: Simulations of convective storms in hurricane environments. Preprints, *16th Conf. on Severe Local Storms,* Kananaskis Park, AB, Canada, Amer. Meteor. Soc., 334–339.

——, 1991: Bouyancy and shear characteristics of hurricane-tornado environments. *Mon. Wea. Rev.,* **119,** 1954–1978.

——, and M. L. Weisman, 1996: Simulations of shallow supercell storms in landfalling hurricane environments. *Mon. Wea. Rev.,* **124,** 408–429.

——, K. R. Knupp, and W. L. Snell, 1993: Observations of tornadic storms and rainbands within Hurricane Andrew's remnants. Preprints, *17th Conf. on Severe Local Storms,* St. Louis, MO, Amer. Meteor. Soc., 272–276.

Novlan, D. J., and W. M. Gray, 1974: Hurricane spawned tornadoes. *Mon. Wea. Rev.,* **102,** 476–488.

OFCM, 1991: WSR-88D products and algorithms. *Federal Meteorological Handbook 11*: Part C, Interim Version One, FCM-H11C-1991, 210 pp. [Available from National Climatic Data Center, 151 Patton Ave., Asheville, NC 28801.]

OSF, 1995: WSR-88D operators guide to mesocyclone recognition and diagnosis. Operational Support Facility (OSF/OTB), Norman, OK, 111 pp. [Available from Operational Support Facility, Operations Training Branch, 3200 Marshall Ave., Suite 202, Norman, OK 73072.]

Powell, M. D., 1982: The transition of the Hurricane Frederic boundary-layer wind field from the open Gulf of Mexico to landfall. *Mon. Wea. Rev.,* **110,** 1912–1932.

——, 1988: Boundary layer structure and dynamics in outer hurricane rainbands. Ph.D. dissertation, The Florida State University, 227 pp. [Available from Department of Meteorology, The Florida State University, Tallahassee, FL 32306.]

Przybylinski, R. W., 1995: The bow echo: Observations, numerical simulations, and severe weather detection methods. *Wea. Forecasting,* **10,** 203–218.

Snell, W. L., and E. W. McCaul Jr., 1993: Doppler signatures of tornadoes spawned by Hurricane Andrew near Montgomery, Alabama. Preprints, *26th Radar Meteorology Conf.,* Norman, OK, Amer. Meteor. Soc., 80–82.

Spratt, S. M., and A. J. Nash, 1995: Central Florida WSR-88D observations and NWSO operations during Tropical Cyclones Alberto, Beryl and Gordon (1994). Preprints, *17th Conf. on Hurricanes and Tropical Meteorology,* Miami, FL, Amer. Meteor. Soc., 298–300.

Stewart, S. R., and S. W. Lyons, 1996: A WSR-88D radar view of Tropical Cyclone Ed. *Wea. Forecasting,* **11,** 115–135.

Vescio, D. M., S. J. Weiss, and F. P. Ostby, 1995: Tornadoes associated with Tropical Storm Beryl. Preprints, *21st Conf. on Hurricanes and Tropical Meteorology,* Miami, FL, Amer. Meteor. Soc., 469–471.

Wakimoto, R. M., and P. G. Black, 1994: Damage survey of Hurricane Andrew and its relationship to the eyewall. *Bull. Amer. Meteor. Soc.,* **75,** 189–200.

Weisman, M. L., and E. W. McCaul Jr., 1995: Simulations of shallow supercells in landfalling hurricane environments. Preprints, *27th Conf. on Radar Meteorology,* Vail, CO, Amer. Meteor. Soc., 428–430.

Weiss, S. J., 1985: On the operational forecasting of tornadoes associated with tropical cyclones. Preprints, *14th Conf. on Severe Local Storms,* Indianapolis, IN, Amer. Meteor. Soc., 293–296.

——, 1987: Some climatological aspects of forecasting tornadoes associated with tropical cyclones. Preprints, *17th Conf. on Hurricanes and Tropical Meteorology,* Miami, FL, Amer. Meteor. Soc., 160–163.

——, and F. P. Otsby, 1993: Synoptic and mesoscale environment associated with severe local storms produced by Hurricane Andrew. Preprints, *17th Conf. on Severe Local Storms,* St. Louis, MO, Amer. Meteor. Soc., 267–271.

Willoughby, H. E., and P. G. Black, 1996: Hurricane Andrew in Florida: Dynamics of a disaster. *Bull. Amer. Meteor. Soc.,* **77,** 543–549.

Zubrick, S. M., and J. D. Belville, 1993: WSR-88D doppler radar observations of weak tornadoes over the mid-Atlantic associated with the remnants from Andrew. Preprints, *17th Conf. on Severe Local Storms,* St. Louis, MO, Amer. Meteor. Soc., 696–701.